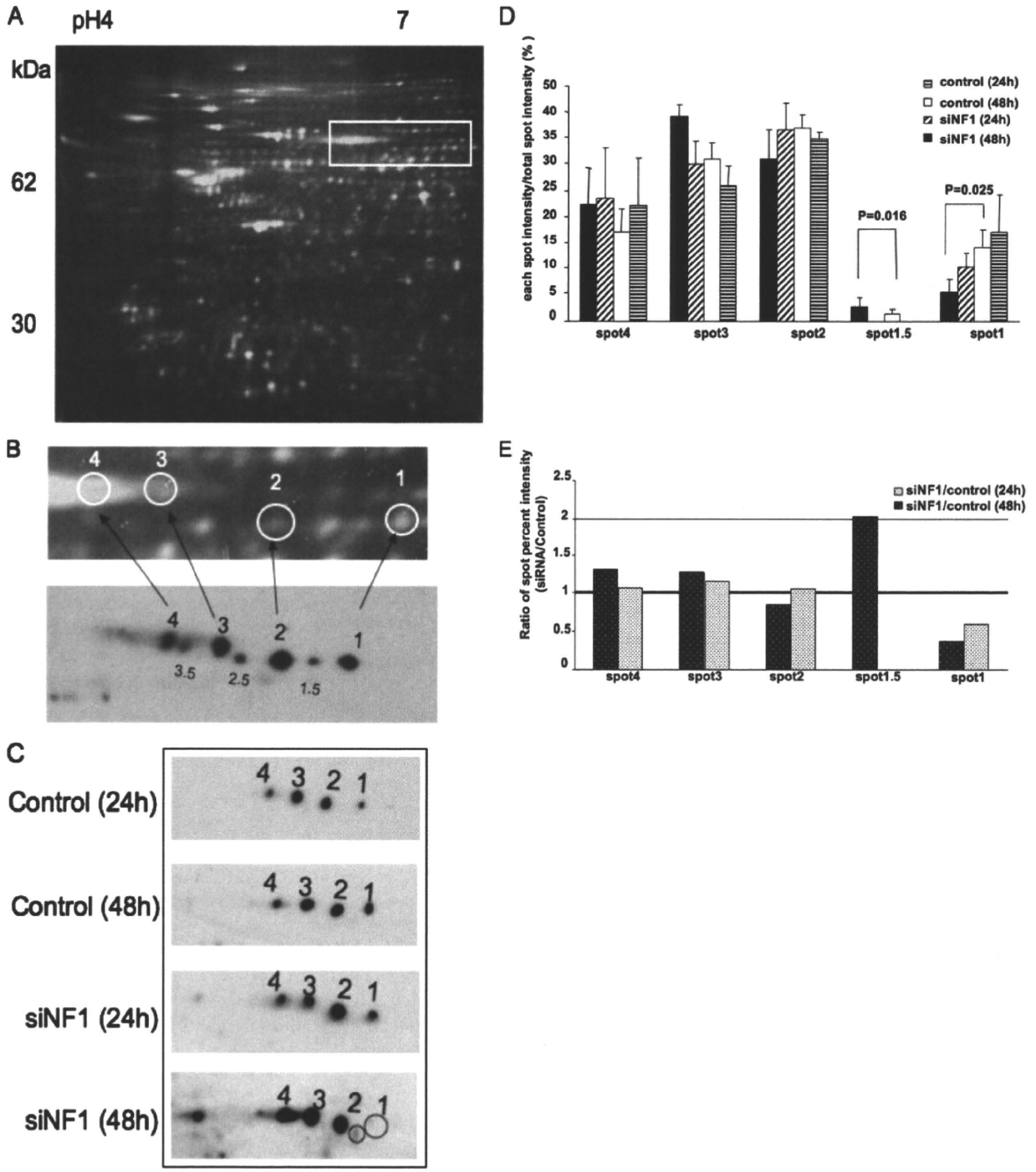

FIGURE 4. **Comparative two-dimensional PAGE analysis of PC12 cells transfected with NF1 siRNA or control siRNA.** *A*, two-dimensional DIGE analysis of PC12 cells transfected with NF1 siRNA (*red*) *versus* control siRNA (*green*). Cellular proteins prepared from PC12 cells transfected with NF1(249) siRNA and control siRNA were labeled with Cy5 (*red*) and Cy2 (*green*), respectively. Two-dimensional patterns (13 × 13 cm) were scanned with Typhoon 9400 and analyzed by Progenesis hands-free analysis. Suppression of NF1 expression by siRNA lead to alteration of the two-dimensional DIGE pattern in PC12 cells. The *inset* indicates the position enlarged in *B*. *B*, identification of CRMP-2 protein spots by two-dimensional Western analysis with anti-CRMP-2 antibodies. *Upper panel* shows two-dimensional DIGE pattern of CRMP-2 enlarged from the *inset* in *A*. *Lower panel* shows CRMP-2 protein spot pattern in two-dimensional Western blotting with anti-CRMP-2 antibodies. Protein spots corresponding to spots 1, 1.5, 2, 2.5, 3, 3.5, and 4 all showed positive against anti-CRMP-2 antibodies. *C–E*, comparison of protein spot intensities of CRMP-2 in PC12 cells transfected with NF1 siRNA *versus* control siRNA. PC12 cells were transfected with NF1(249) siRNA or control siRNA, stimulated with NGF, and harvested after 24 or 48 h of NGF treatment. Each cellular lysate was subjected to two-dimensional Western analysis (7 × 7 cm) using anti-CRMP-2 antibodies (*C*). Percent ratios of each spot intensity in total spot intensity were indicated in each histogram (*D*), and ratios of spot percent intensities of NF1 siRNA *versus* control siRNA of each protein spot 1, 1.5, 2, 3, and 4 in total spot intensity of CRMP-2 were calculated and indicated in each histogram (*E*). The spot intensities of spot 1.5 in both of NF1 siRNA and control cells after 24 h of NGF treatment were below the detection limit. The data were obtained from four separate identical experiments, and these averages, and the significant coefficient of correlation values less than 0.05, are shown in each histogram. *Error bars* represent S.E.

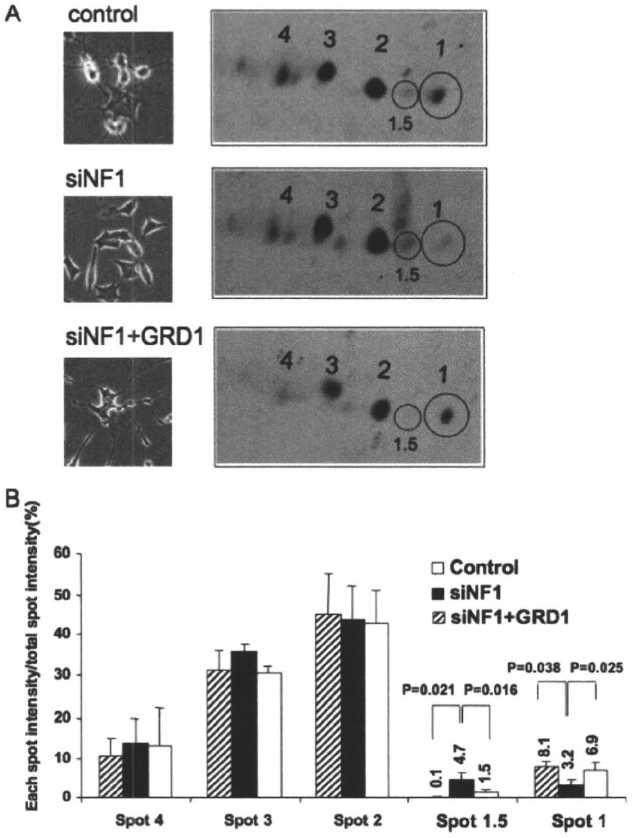

FIGURE 5. **Rescue experiment with NF1-GRD on the neurite outgrowth inhibition and changes of CRMP-2 two-dimensional pattern by NF1-siRNA in PC12 cells.** *A*, control siRNA and NF1(249) siRNA were transfected separately or co-transfected with NF1 (GRD) type 1 into PC12 cells before treating with NGF for 24 h. After 48 h of NGF treatment, cellular morphologies were observed with the phase-contrast microscope (×100) and subjected to the analysis with two-dimensional immunoblotting using anti-CRMP-2 antibody. *B*, comparison of each spot intensity for CRMP-2 after the transfection of NF1 siRNA and NF1 GRD. The *histograms* show the percentage of each spot intensity in total spot intensity of CRMP-2s in individual samples. The intensity of each sample was obtained by two-dimensional Western blotting using anti-CRMP-2 antibody followed by Cy5-labeled secondary antibody. The data were obtained from the average results of the four separate identical experiments, and the significant coefficient of correlation values less than 0.05 are shown in each histogram. *Error bars* represent S.E. of three sets of those experiments.

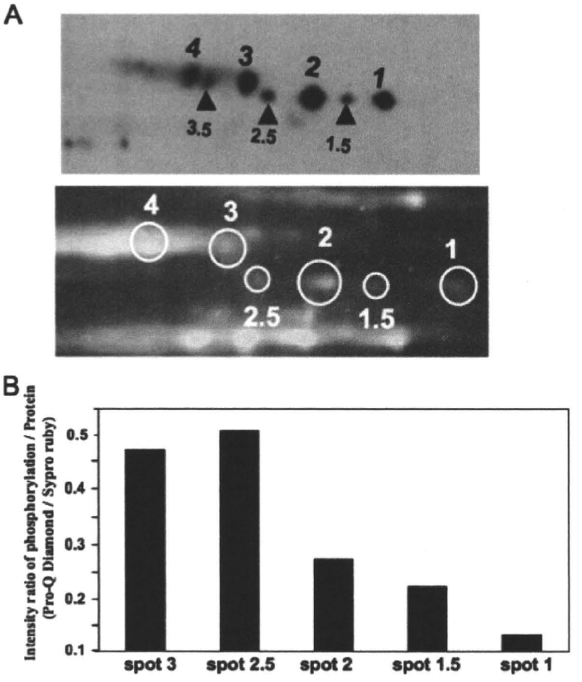

FIGURE 6. **Semi-quantitative two-dimensional PAGE analysis of CRMP-2 phosphorylation using ProQuant Diamond staining.** *A*, phosphorylated CRMP-2s were sequentially shifted to the acidic pI region in two-dimensional gels. Phosphorylated CRMP-2 separated on two-dimensional gels were stained with ProQuant Diamond (*red*) and SYPRO Ruby (*green*), scanned with Typhoon 9400, and merged, respectively. *B*, ratios of each spot intensity stained with ProQuant Diamond for phosphoprotein *versus* SYPRO Ruby for protein. The *y* axis shows the ratio of fluorescent intensities of spots 1, 1.5, 2, 2.5, and 3 obtained from ProQuant Diamond staining *versus* SYPRO Ruby staining. The ratios for spots 3.5 and 4 were not calculated because other unknown protein spots crossed over on those spots and caused difficulties for the calculation.

lower intensities (Fig. 7*L*) or very low reactivity against anti-phospho-Thr^{514} CRMP-2 antibody (Fig. 7*M*), suggesting that spot 3 could possess the phosphorylation site of Thr^{514} by GSK3-β and that spot 4 could possibly have another phosphorylation site such as Thr^{518} or Thr^{509} as reported (17), in addition to Thr^{514}. It is well known that a GSK-3β priming kinase such as Cdk5 is necessary for the GSK-3β phosphorylation of CRMP-2. Thus, we treated the cells with or without a Cdk5 inhibitor, purvalanol A, and the effect on the two-dimensional pattern of CRMP-2 was analyzed. As shown in Fig. 7, *F* and *G*, there were significant decreases in the spot intensities of spots 2–4, and remarkable increases in the intensities of spots 1 and 1.5 in the presence of purvalanol. To confirm these spot shifts were caused by the CDK5 inhibition, the same samples used for Fig. 7, *F* and *G*, were subjected to two-dimensional Western analysis using the specific antibody against Cdk-5-phosphoryl-ated CRMP-2 (anti-phospho-Ser^{522} CRMP-2 antibody). The anti-phospho-Ser^{522} CRMP-2 antibody significantly reacted with spot 2, 2.5, 3, 3.5, and 4 in the absence of the inhibitor (Fig. 7*H*), whereas these reactive spots almost disappeared in the presence of purvalanol (Fig. 7*I*). To confirm our speculation that spot 1 is a real nonphosphorylated form of CRMP-2, the cellular CRMP-2 spot 1 was analyzed by ProQuant Diamond and SYPRO Ruby staining, after Cdk5 inhibitor treatment that significantly amplified the spot 1 intensity in a two-dimensional Western blot (Fig. 7*G*). The intensity of SYPRO Ruby protein staining of spot 1 was increased with Cdk5 inhibitor more than five times, but the intensity of phospho-staining by ProQuant Diamond was not increased compared with those in the control condition, suggesting that spot 1 is a nonphosphorylated CRMP-2 (supplemental Fig. S2). These results strongly indicate that spot 2, which shifted from spot 1, could have a Cdk5 phosphorylation site of Thr^{522} that acts as a priming phosphorylation site for GSK-3β. We also deduced that spots 3 and 4 could both have a phosphorylation site of Thr^{522} in addition to the phosphorylation site of Thr^{514}. The spot 1.5 increased in intensity, whereas spots 2.5 and 3.5 decreased in intensity after purvalanol A treatment suggested that Rho kinase-related spots 2.5 and 3.5 might be involved in the phosphorylation by Cdk5 and/or that the Cdk inhibition caused the Rho kinase activation.

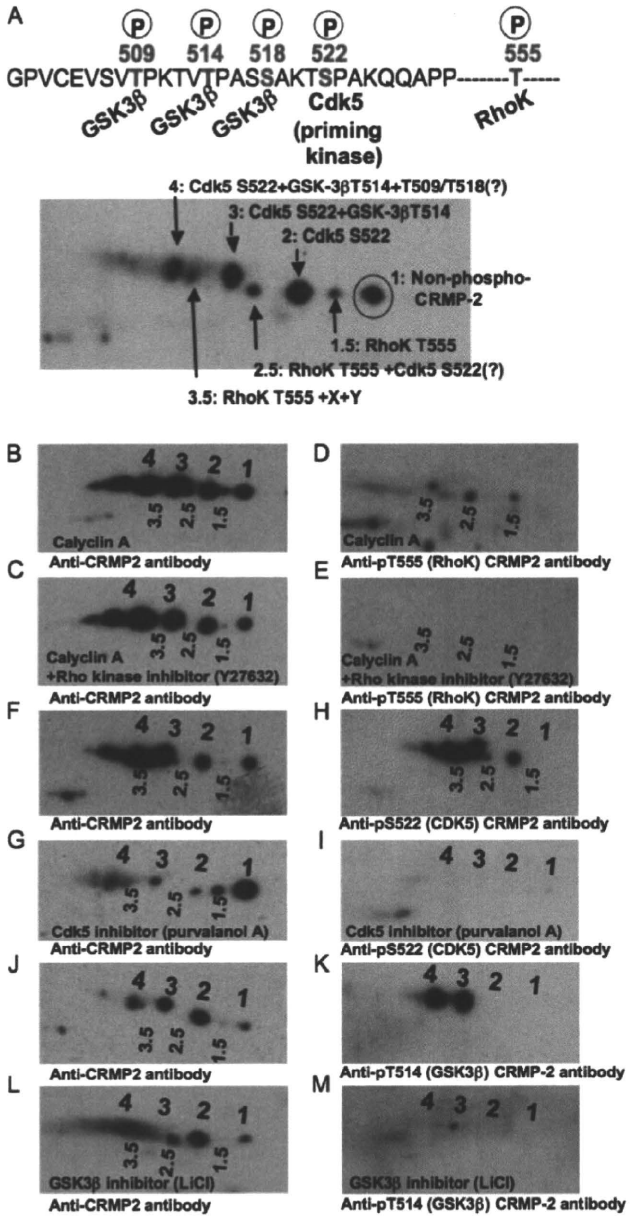

FIGURE 7. **Identification of CRMP-2 spots phosphorylated and shifted on two dimensions by the specific kinases in PC12 cells.** *A*, postulated phosphorylation sites on the amino acid sequence of CRMP-2 (Thr^{509}, Thr^{514}, Ser^{518}, Ser^{522}, and Thr^{555}) and the specific kinases (GSK3β, Cdk5, and Rho kinase) for CRMP-2. *B–E*, identification of CRMP-2 phosphorylated spots by Rho kinase on two dimensions by using Rho kinase inhibitor and anti-phospho-Thr^{555} (Rho kinase) CRMP-2 antibody. After 48 h of NGF treatment, cells were incubated without (*B* and *D*) or with 10 μM Rho kinase inhibitor (Y27632) (*D* and *E*) for 1 h at 37 °C in a CO_2 incubator, and then for 30 min with the addition of calyculin-A (10 μM) in a serum-free condition. After washing, cells were lysed with lysis buffer A and subjected to analysis with two-dimensional immunoblotting using anti-CRMP-2 antibody (*B* and *C*) or anti-phospho-Thr^{555} (Rho kinase) CRMP-2 antibody (*D* and *E*). *F–I*, identification of CRMP-2-phosphorylated spots by Cdk5 on a two-dimensional gel using Cdk5 inhibitor and anti-phospho-Ser^{522} (Cdk5) CRMP-2 antibody. After 48 h of NGF treatment, cells were incubated with (*G* and *I*) or without (*F* and *H*) 10 μM Cdk5 inhibitor (purvalanol A) for 24 h at 37 °C in a CO_2 incubator, and subjected to the analysis with two-dimensional immunoblotting using anti-CRMP-2 antibody (*F* and *G*) or anti-phospho-Ser^{522} (Cdk5) CRMP-2 antibody. *J–M*, identification of CRMP-2-phosphorylated spots by GSK-3β on two dimensions using anti-phospho-Thr^{514} (GSK-3β) CRMP-2 antibody and GSK-3β inhibitor. After 48 h of NGF treatment, cells were incubated with (*L* and *M*) or without (*J* and *K*) GSK-3β inhibitor LiCl (30 mM) for 24 h at 37 °C in a CO_2 incubator, and subjected to analysis with two-dimensional immunoblotting using anti-CRMP-2 antibody (*J* and *L*) or anti-phospho-Thr^{514} (GSK-3β) CRMP-2 antibody (*K* and *M*).

Suppression of Neurofibromin by NF1 siRNA Up-regulated Cdk5, GSK-3β, and RhoK Phosphorylation of CRMP-2 in PC12 Cells after NGF Treatment—It is clearly evident that intensity changes in the protein spots of CRMP-2 caused by kinase inhibitor treatments of PC12 cells reflect the alteration of CRMP-2 phosphorylation status. We speculated that CRMP-2 phosphokinases could be regulated by neurofibromin during neurite outgrowth in PC12 cells. To understand the role of neurofibromin in cellular phosphorylation of CRMP-2 and its significances for neurite outgrowth, we analyzed the effects of kinase inhibitors on CRMP-2 phosphorylation as well as phenotypic changes in PC12 cells after treatment with NF1 siRNA.

PC12 cells stimulated with NGF after suppression of neurofibromin by siRNA were treated with Rho kinase inhibitor (Y27632), and the CRMP-2 two-dimensional Western patterns were analyzed semi-quantitatively. As shown, Fig. 8, *A*, *panel c*, and *B*, *spot 1.5*, designated as a Rho kinase-phosphorylated spot (phospho-Thr^{555}), significantly disappeared. Interestingly, the decrease in spot 1.5 intensity occurred in parallel with a decrease in the intensity of spot 2 (phosphorylated CRMP-2 (phospho-Ser^{522}) by Cdk). In addition, the intensities of spots 3 and 4 (phosphorylated CRMP-2 (phospho-Thr^{514}) by GSK-3β in addition to Cdk5 phosphorylation at phospho-Ser^{522}) were increased in the Rho kinase inhibitor-treated cells combined with NF1-siRNA treatment, compared with the control cells. At the same time, we observed the effect of Rho kinase inhibitor on the neurite retraction caused by NF1-siRNA. RhoK inhibitor showed some effects on the neurite recovery as shown in Fig. 8*A*, *panel c* (*left* and *middle panel*); however, the effects on the extension pattern of neurites and the cellular shape were different (shorter filopodia and a round cell body as shown in Fig. 8*A*, *panel c*) from those of control cells. These results suggest that NF1 siRNA increases the Rho kinase-related phosphorylation of CRMP2 and that combining treatment by Rho kinase inhibitor with NF1 siRNA affects both Rho kinase as well as Cdk5/GSK-3β phosphorylation of CRMP2. These CRMP-2 phosphorylation changes on CRMP-2 may reflect the incomplete neurite recovery in RhoK inhibitor treatment.

On the other hand, the combined treatment of Cdk5 inhibitor (purvalanol A or olomoucine) with NF1 siRNA was significantly effective in decreasing the intensities of spots 2–4 (Fig. 8*A*, *panel d*, and *B*, and supplemental Fig. S3), which were designated as Cdk5 and GSK-3β-related phospho-CRMP-2 respectively. In this condition, the intensity increase of spot 1 (nonphosphorylated CRMP-2) in Cdk5 inhibitor-treated cells was also significant. The intensity of spot 1.5, which is related to Rho kinase, was also increased after Cdk5 inhibitor and NF1 siRNA treatment, suggesting the Cdk5 involvement of spot 1.5 as shown in Fig. 7*G*, Fig. 8, *A*, *panel d*, and *B*, and supplemental Fig. S3, *B* and *C*. These effects dramatically reflected the neurite extension rescuing the retraction by NF1 siRNA as shown in Fig. 8*A*, *panel d*, and supplemental Fig. S3, *B* and *C*, suggesting that NF1 siRNA-related spot 1 intensity decrease and neurite

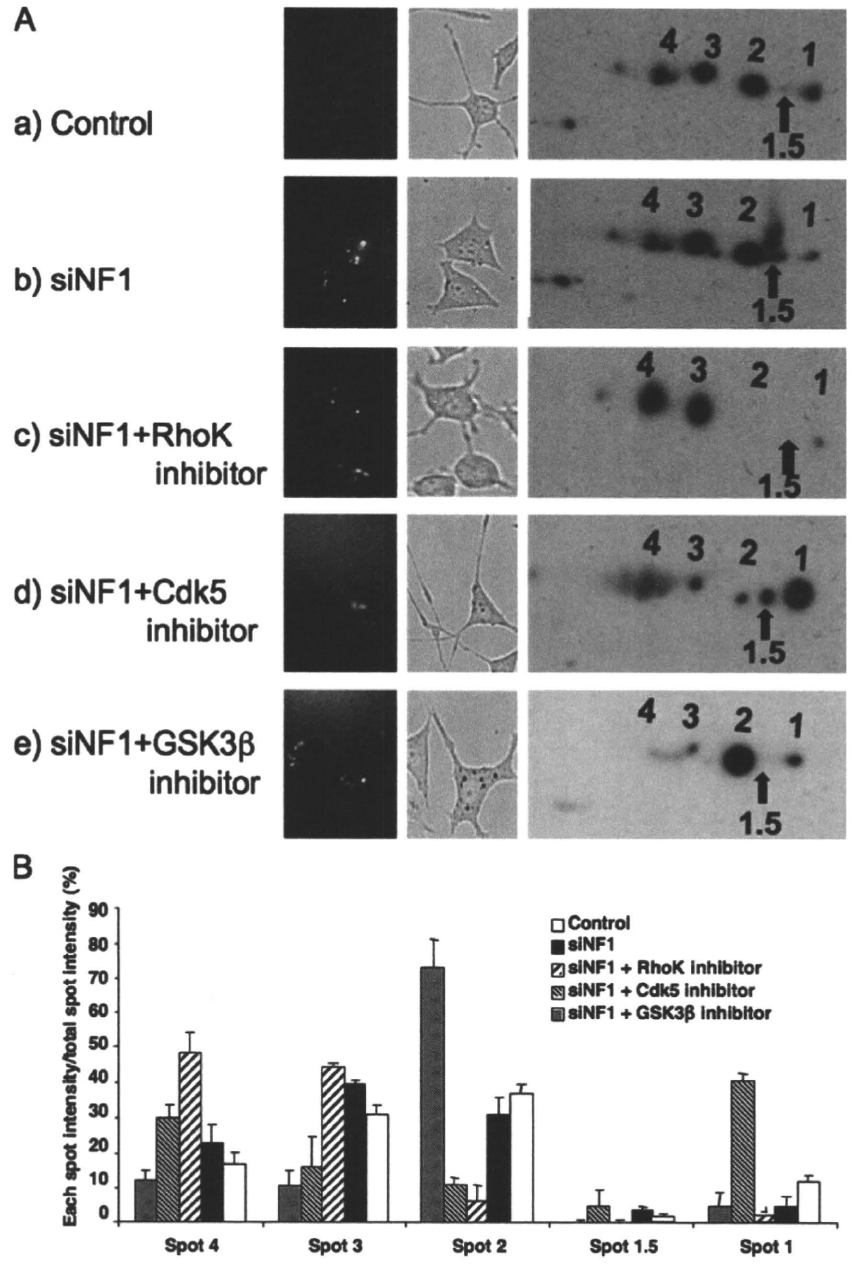

FIGURE 8. **Effects of Rho kinase, Cdk5, and GSK-3β inhibitor on NF1 siRNA-induced CRMP-2 phosphorylation and neuronal retraction in PC12 cells.** *A, right panel,* comparison of the CRMP-2 spot patterns in the NF1 siRNA or control siRNA-treated cells in the presence or absence of Rho kinase, Cdk5, and GSK-3β inhibitors. After 48 h of transfection of NF1 siRNA (*panels b–e*) or control siRNA (*a*) to the NGF-treated PC12 cells, cells were treated with (*panels c–e*) or without (*panels a* and *b*) 10 μM Rho kinase inhibitor (Y27632) (*panel c*), 10 μM Cdk 5 inhibitor (purvalanol A) (*panel d*), or 30 mM GSK-3β inhibitor (LiCl) (*panel e*) and subjected to two-dimensional immunoblotting analysis with anti-CRMP-2 antibody, as described in Fig. 7 and under "Experimental Procedures." *Middle panel,* phase contrast photograph of each cells treated with kinase inhibitors. *Left panel,* fluorescent NF1 siRNA incorporated into the cells. *B,* comparison of each spot intensity for CRMP-2 patterns in the cells that were treated with the same conditions of *A*. The *histograms* show the percentage of each spot intensity per total spot intensity obtained from the average of three separate identical experiments of two-dimensional immunoblotting analysis. *Error bars* represent S.E.

retraction could be mainly caused by Cdk5 activation. In the area of spot 4, which represents more than three phosphorylation sites of CRMP-2, a relatively broad increase in intensity was detected and labeled as Cdk5 inhibitor effects with an unknown reason.

Finally, the effects of combined treatment of GSK-3β inhibitor (LiCl) with NF1 siRNA was analyzed. The result revealed that LiCl treatment was dramatically effective in decreasing the intensities of spots 3 and 4 (Fig. 8, *A, panel e,* and *B*), which were designated as both GSK-3β (phospho-Thr^{514}), and Cdk5 (phospho-Ser^{522})-related phospho-CRMP-2. However, the effect of LiCl on spot 1 was not significant, and its morphological effect of rescuing the neurite retraction was small (Fig. 8*A*, *panel e*). These results demonstrate that individual treatment by the GSK-3β inhibitor stops further sequential phosphorylation of the CRMP-2 spot 2 to spots 3 and 4, but it has little effect functionally on neurite retraction in this system.

From these results, it is indicated that both the NF1 siRNA-related decrease in intensity of spot 1 and the increase in intensity of spot 1.5 are related to the complemental activation of Cdk5, GSK-3β, and the Rho kinase, as well as their phosphorylation of CRMP-2. However, neurofibromin-related neurite regulation, in association with CRMP-2 phosphorylation, may be mainly controlled via the regulation of Cdk5 kinase activity, which strongly controls the intensity of spot 1, the nonphosphorylated active form of CRMP-2.

DISCUSSION

In this study, we demonstrated a novel function of neurofibromin in neurite outgrowth of PC12 cells comprising regulation of CRMP-2 phosphorylation via direct and indirect association with CRMP-2 (supplemental Fig. S5). CRMP-2 was identified as a neurofibromin-binding protein using newly developed proteomic affinity mapping methods. Neurofibromin directly interacts with the active (nonphosphorylated) form of CRMP-2, but not with the inactive (phosphorylated) form of CRMP-2, via the neurofibromin CTD. Immunocytochemical analysis showed that neurofibromin and CRMP2 are co-localized especially in the distal tips and branches along the neurites, which are recognized as major CRMP-2 action sites (18) in differentiated PC12 cells. Depletion of neurofibromin in PC12 cells with NF1

siRNA up-regulated the inactivation of CRMP-2 by phosphorylation, which induced neurite retraction of the cells. The phosphorylation of CRMP-2 is regulated with several kinases, such as Cdk5, GSK-3β, and Rho kinase. Here we present evidence that the phosphorylation of CRMP-2 by these kinases may be regulated by neurofibromin via the direct interaction/complex formation with CRMP-2, and by indirect regulation of these kinase cascades in PC12 cells during neurite outgrowth after NGF treatment.

Previously, we found that time-dependent increases in the GAP activity of cellular neurofibromin (NF1-GAP) were detected after NGF stimulation in PC12 cells, and these increases were correlated with the down-regulation of Ras activity during neurite elongation (6). Interestingly, when cellular NF1-GAP activity was inhibited with dominant-negative (DN) forms of NF1-GRD type I, neurite extension of PC12 cells was significantly inhibited. This correlated with prolonged Ras activation and longer stimulation by NGF (6).

Similar results were obtained in the present study using NF1 siRNA, which caused depletion of neurofibromin and significant inhibition of neurite outgrowth. Forty eight hours of observation with a time-lapse microscope directly following NGF addition showed that PC12 cells transfected with NF1 siRNA displayed weak and short neurite extension, which quickly resulted in retraction (Fig. 3 and supplemental movies 1 and 2). Phenotypic changes were also observed in the rat embryonic hippocampal primary neuron whose axonal extension was significantly reduced after treatment with NF1 siRNA,[3] as we observed a similar result in previous studies with using GRD-DN overexpression (6). The rescue experiment performed by overexpressing the high NF1-GAP activity FLAG-GRD type I (6) was successful in both changing neurite outgrowth and the CRMP-2 phosphorylation pattern (Fig. 5, *A* and *B*). Thus, it could be concluded that cellular Ras regulation by NF1-GAP is one of the most important events in neuronal development, although another function of neurofibromin in addition to NF1-GAP activity may also be part of this mechanism.

Most of the *NF1* mutations are nonsense, frameshift, or truncating mutations leading to premature termination codons (19, 20), and a relatively high frequency of the mutations have been reported downstream of the GRD in the C-terminal region. This suggested that the neurofibromin C terminus is a crucial region in regulating neurofibromin function. In our previous study, we identified several functional proteins, such as 14-3-3s (14) and DDAH (10), that bound to the C-terminal NF1 and affected the GAP activity of neurofibromin, suggesting that the C-terminal region of neurofibromin could be a regulatory domain for GRD activity. In this context, identification and analysis of cellular proteins that are bound to C-terminal neurofibromin are thought to be crucial to elucidate the biological significance of neurofibromin.

In this study, at least 58 proteins associating with neurofibromin (Table 1) were identified semi-quantitatively with (iTRAQ) using micro-affinity columns and NanoLC ESI/MALDI-MS/MS analysis. These proteins contained several neuronal regulating proteins, including not only previously known but also novel proteins, such as CRMP-2, which is known as an axon regulatory cargo protein. This information moved us to analyze the mutual association of CRMP-2 and neurofibromin in conjunction with neuronal function.

Collapsin-response mediator proteins are a family of cytosolic proteins developmentally regulated in the nervous system (21–24), which are assumed to mediate intracellular responses to collapsin (25). Collapsin-response mediator proteins have significant homology with the product of *unc*-33 in *Caenorhabditis elegans*, the mutation of which results in abnormal axon outgrowth (26–28). CRMP-2 directly binds to kinesin light chain (KLC1) and tubulin, resulting in a trimeric complex that regulates tubulin transport to the distal part of the growing axon (29). Analogous to the CRMP-2-tubulin interaction, it is speculated that neurofibromin could be a new CRMP-2-related cargo or complex protein that functions as a regulator of the axon formation complex. It was reported that interaction between CRMP-2 and tubulin was altered by CRMP-2 phosphorylation by Cdk5, GSK-3β (30), and by Rho kinase (11). In our study, the interactions of neurofibromin, CRMP-2, and tubulin were confirmed with immunoprecipitation assay using each of their respective antibodies, and it was found that neurofibromin and tubulin could bind strongly to the nonphosphorylated form of CRMP-2, as we expected (Fig. 1, *C* and *D*).

In general, the phosphorylation of CRMP-2 has been analyzed using one-dimensional Western blotting, after which it has been assessed whether the band for CRMP-2 shifts up or not. Our strategies used in this study, such as two-dimensional DIGE combined with a specific staining for phosphorylated proteins (ProQuant Diamond) and two-dimensional Western blotting using specific antibodies, could be an original method to identify a series of CRMP-2 protein spots with varying types of phosphorylation. We identified the specific phosphorylation sites of CRMP-2 by Rho kinase, Cdk5, and GSK-3β in PC12 cells and demonstrated that the neurite retraction is exacerbated by the combinatorial up-regulation of CRMP-2 phosphorylation. As we summarized in Figs. 7 and 8, CRMP-2 phosphorylation is represented starting with a shift in intensity from spot 1 to spot 2 caused by the up-regulation of Cdk5. Spot 2 contains the first phosphorylation site by Cdk5 (Ser^{522}), followed by GSK-3β activation adding the second phosphorylation (Thr^{514}) on spot 3, and the third phosphorylation (possibly Thr^{518}, Thr^{509}, or another) on spot 4. In a parallel manner, spot 1.5, corresponding to Rho kinase-related phospho-CRMP-2 (Thr^{555}), is revealed and followed by the other two phosphorylations on spots 2.5 and 3.5. It is reasonable to speculate that the regulation of neurofibromin-related Ras signaling is necessary for CRMP-2 phosphorylation and neurite outgrowth, because these changes in the spot intensities were rescued with the overexpression of NF1-GRD (6) (Fig. 5).

When we focus on the intensity alteration of spot 1, an active form of CRMP-2 (nonphosphorylated form), a part of the mechanism of neurofibromin-dependent neurite regulation could be simply interpreted in association with CRMP-2 function. First, this active CRMP-2 can form a complex with neurofibromin to maintain the activity to process the neurite outgrowth with NGF treatment, where NF1-GAP may contribute to slow the Ras signal cascade related to CRMP-2 phosphorylation such as MAPK-Cdk5-GSK-3β, Rho-RhoK, and others. Second, neurofibromin depletion by siRNA treatment signifi-

[3] N. Araki, S. Patrakitkomjorn, N. Arimura, and K. Kaibuchi, unpublished observations.

cantly decreased spot 1 intensity and increased the Cdk5, GSK-3β RhoK-dependent phosphorylation on CRMP-2, and this was correlated with the neurite retraction of PC12 cells. Third, the decrease of the CRMP-2 spot 1 and the neurite retraction were significantly rescued with NF1-GAP domain overexpression (Fig. 5) or Cdk5 inhibitor treatment (Fig 8*A*, *panel d*, and supplemental Fig. S3). Thus, we speculate that the increase of nonphosphorylated CRMP-2 (spot 1) is most important for the neurite outgrowth, and that this was regulated with neurofibromin by inhibiting both Cdk5 activity and CRMP-2 phosphorylation (supplemental Fig. S5).

Concerning spots 2–4, the ratio of their combined spot intensity (CSI) to the total spot intensity (TSI) (spots 1–4) was significantly increased after NF1 siRNA treatment because spot 1 decreased in a statistically significant manner, suggesting that the activation of Cdk5 and that of GSK-3β thereafter may be controlled by neurofibromin depletion. Inhibition of neurite outgrowth was correlated with the increases in the CSI ratio, and phenotypic changes were rescued by NF1-GAP domain overexpression or Cdk5 inhibitor treatment. Nevertheless, only a partial effect was observed with the GSK-3β inhibitor, which magnified the significant increase of spot 2 and the decrease of spots 3 and 4 (Fig. 8), suggesting that the main factor of the NF1-related regulation of neurite outgrowth and CRMP-2 phosphorylation may be Cdk5, but also GSK-3β may function as a player working with its priming kinase Cdk5 to accelerate the phosphorylation of CRMP2 and cause the decrease of the active form of CRMP-2 (spot 1), thereby relating indirectly to the neurite regulation in this system.

On the other hand, spot 1.5 (RhoK-phosphorylated CRMP-2 (phospho-Thr^{555}) was significantly increased after NF1 siRNA treatment, suggesting that the activation of RhoK is controlled by the neurofibromin depletion. Inhibition of neurite outgrowth was also correlated with the increase in spot 1.5 intensity, and these phenotypic changes were rescued by NF1-GAP domain overexpression or RhoK inhibitor (although the effect of RhoK inhibitor for neurite recovery was partial) as shown in Figs. 5 and 8. This suggested that the activation of RhoK was at least controlled by the neurofibromin depletion, and some part of the NF1-related regulation of neurite outgrowth and CRMP-2 phosphorylation could involve RhoK regulation.

After Cdk5 inhibitor treatment, the increase in spot 1.5 by NF1 depletion was more significant and reproducible (Fig. 8). This was speculated that increase of spot 1.5 is partly caused by the shift and decrease of spots 2.5 and 3.5 after Cdk 5 inhibitor treatment. Because they have Cdk phosphorylation site in addition to the Rho kinase site, their shift to the spot 1.5 position by the inhibition of Cdk5 resulted in the increase of the intensity of spot 1.5. Spots 2.5 and 3.5 were also increased after NF1 depletion and rescue experiments with NF1-GAP domain overexpression or RhoK inhibitor looked effective in decreasing those spot intensities, although these spots were originally too small to calculate statistically. Thus, in this study we do not discuss in depth the intensity changes of 2.5 and 3.5 spots, and their relation to the neurite outgrowth. The NF1-GAP-related regulatory signals in neuronal cells such as Ras-MAPK, Ras-PI3K (6), and Rho-RhoK/ROCK-LIMK (9) have been reported previously. In this study, we are the first to demonstrate that the phosphorylations of CRMP-2 by Cdk5, GSK-3β, and Rho/Rho kinase, which are regulated with neurofibromin, play a role in the neurite outgrowth of PC12 cells (supplemental Fig. S5).

Concerning the functional association of Rho/Rho kinase to cellular neurofibromin, in our previous study we demonstrated that neurofibromin depletion by NF1 siRNA activates cell motility by regulating the dynamics and reorganization of actin filaments via the Rho-RhoK/ROCK-LIMK2-cofilin pathway (9). Recently, several lines of evidence have also implicated the Rho kinase/ROCK-LIMK-cofilin pathway in the regulation of axon growth and guidance in neuronal cells (31–35). Although CRMP-2 phosphorylation by Rho kinase has been reported during the lysophosphatidic acid-induced growth cone collapse in neurons, this could be the first study to implicate the Rho-Rho kinase pathway as causing neurite retraction in PC12 cells after neurofibromin (NF1-GAP) depletion.

Cdk5 is also reported as being activated mainly in post-mitotic cells such as neurons (36) and is suggested to play important roles in neurite outgrowth (37) and neuron migration (38). Cdk5 also modulates protein kinase reactions such as Rac-dependent phosphorylation of p21, which results in modification of the actin cytoskeleton (39). Because the Ras-MAPK signal transcriptionally up-regulates p35 protein, which is an active binding unit for Cdk5, our demonstration of the up-regulation of Cdk5 via NF1-GAP depletion and Ras activation seems reasonable (supplemental Fig. S5).

On GSK-3β function, the report showing that Ras-PI3K-AKT signal activation causes the inactivation of GSK-3β and enhances neurite outgrowth rates in PC12 cells (40–42) looked controversial, considering our results showed that Ras signal activation caused by NF1-GAP depletion resulted in GSK-3β activation, up-regulation of CRMP-2 phosphorylation, and neurite retraction. However, there are several reports strongly demonstrating that GSK-3β is activated via the activation of Cdk5 as a priming kinase (17), and also via Rho-related signal activation (31), supporting our speculation that activation of Cdk5 and Rho/RhoK after neurofibromin depletion can affect the up-regulation of GSK-3β (supplemental Fig. S2).

The direct evidence on the relationship between neurofibromin binding to CRMP-2 and neuronal differentiation could be important to understand the mechanism of this study more correctly. To obtain the information related to this, NF1-CTD was overexpressed in PC12 cells to inhibit the cellular binding of neurofibromin to CRMP-2. After NGF stimulation of PC12 cells, the GFP-NF1-CTD fluorescence was detected successfully in the cells, and their neurite outgrowth was significantly inhibited compared with that of GFP-Mock cells as shown in supplemental Fig. S4. However, in addition to this cellular event, we noticed that the effect of the CTD overexpression on the neurite outgrowth was morphologically different from that in the NF1 siRNA-treated cells. For instance, the GFP-CTD-transfected cells represented a smaller size of the cellular body than those of control cells, and cell detachment was frequently observed. We speculate that the NF1-CTD may work as a regulatory domain for other binding partners, such as tubulins, actin, cofilin, Arp2/3 complex cytoskeletal-organizing proteins, and so on (as shown in Table 1), to collaborate and obtain another cellular function in PC12 cells. Thus, we conclude that

NF1-CTD overexpression could not be a simple "decoy" for the cellular binding of CRMP-2 and neurofibromin but that it could have a more complex function existing in this system to be clarified. Further study will be needed to understand this mechanism underlying neurofibromin functions associated with other binding partners in the neuronal cellular differentiation.

In conclusion, we postulate a novel function of cellular neurofibromin associated with CRMP-2 activity in which it performs two complementary roles (supplemental Fig. S5). First, neurofibromin directly regulates CRMP-2 activation through association, which may protect the phosphorylation sites or change the conformation of CRMP-2 and, in turn, prevent the exposure of CRMP-2 to several kinases such as Rho kinase, Cdk5, and GSK-3β. By the suppression of neurofibromin, the chance of CRMP-2 being exposed to its kinases could be increased. Second, neurofibromin indirectly regulates CRMP-2 by suppressing CRMP-2-phosphorylating kinases. Neurofibromin activity (NF1-GAP) may regulate CRMP-2 phosphokinase activities via the regulation of Ras-related signal pathways, such as MAPK-Cdk5- GSK-3β and Rho-Rho kinase. The suppression of neurofibromin can result in the inhibition of neurite outgrowth via increased activity of Ras signals, which activates kinases involved in CRMP-2 phosphorylation. By using NGF-stimulated PC12 cells as a model, our study has demonstrated a possible cellular function of neurofibromin in neuronal cell differentiation. Further studies based on our findings will shed light on the mechanism of NF1-related neuronal pathogenesis, such as learning disability and memory retardation.

Acknowledgments—We thank Prof. Yoshio Goshima (Department of Molecular Pharmacology and Neurobiology, Yokohama City University Graduate School of Medicine) for providing us anti-phosphorylated CRMP2 (pS522) antibody. We also thank the entire staff of the Tumor Genetics and Biology Department at Kumamoto University for helpful discussion, especially M. Hayashida, K. Cho, M. Junking, A. Silsirivanit, and M. Nagayama for collaborative endeavors; Y. Fukushima, M. Morikawa, and M. Shimono for secretarial assistance; and A. Wilson for manuscript editing. We are also grateful to staff members of the Proteomic Analysis Core System on General Research Core Laboratory, Kumamoto University Medical School, for important contributions to the experiments.

REFERENCES

1. Stephens, K., Riccardi, V. M., Rising, M., Ng, S., Green, P., Collins, F. S., Rediker, K. S., Powers, J. A., Parker, C., and Donis-Keller, H. (1987) *Genomics* **1,** 353–357
2. Cawthon, R. M., Weiss, R., Xu, G. F., Viskochil, D., Culver, M., Stevens, J., Robertson, M., Dunn, D., Gesteland, R., O'Connell, P., and White, R. (1990) *Cell* **62,** 193–201
3. Costa, R. M., Federov, N. B., Kogan, J. H., Murphy, G. G., Stern, J., Ohno, M., Kucherlapati, R., Jacks, T., and Silva, A. J. (2002) *Nature* **415,** 526–530
4. Guo, H. F., Tong, J., Hannan, F., Luo, L., and Zhong, Y. (2000) *Nature* **403,** 895–898
5. Gregory, P. E., Gutmann, D. H., Mitchell, A., Park, S., Boguski, M., Jacks, T., Wood, D. L., Jove, R., and Collins, F. S. (1993) *Somatic Cell Mol. Genet.* **19,** 265–274
6. Yunoue, S., Tokuo, H., Fukunaga, K., Feng, L., Ozawa, T., Nishi, T., Kikuchi, A., Hattori, S., Kuratsu, J., Saya, H., and Araki, N. (2003) *J. Biol. Chem.* **278,** 26958–26969
7. Xu, H., and Gutmann, D. H. (1997) *Brain Res.* **759,** 149–152
8. Li, C., Cheng, Y., Gutmann, D. A., and Mangoura, D. (2001) *Brain Res. Dev. Brain Res.* **130,** 231–248
9. Ozawa, T., Araki, N., Yunoue, S., Tokuo, H., Feng, L., Patrakitkomjorn, S., Hara, T., Ichikawa, Y., Matsumoto, K., Fujii, K., and Saya, H. (2005) *J. Biol. Chem.* **280,** 39524–39533
10. Tokuo, H., Yunoue, S., Feng, L., Kimoto, M., Tsuji, H., Ono, T., Saya, H., and Araki, N. (2001) *FEBS Lett.* **494,** 48–53
11. Fukata, Y., Itoh, T. J., Kimura, T., Menager, C., Nishimura, T., Shiromizu, T., Watanabe, H., Inagaki, N., Iwamatsu, A., Hotani, H., and Kaibuchi, K. (2002) *Nat. Cell Biol.* **4,** 583–591
12. Yoshimura, T., Kawano, Y., Arimura, N., Kawabata, S., Kikuchi, K., and Kaibuchi, K. (2005) *Cell* **120,** 137–149
13. Bollag, G., McCormick, F., and Clark, R. (1993) *EMBO J.* **12,** 1923–1927
14. Feng, L., Yunoue, S., Tokuo, H., Ozawa, T., Zhang, D., Patrakitkomjorn, S., Ichimura, T., Saya, H., and Araki, N. (2004) *FEBS Lett.* **557,** 275–282
15. Byk, T., Dobransky, T., Cifuentes-Diaz, C., and Sobel, A. (1996) *J. Neurosci.* **16,** 688–701
16. Byk, T., Ozon, S., and Sobel, A. (1998) *Eur. J. Biochem.* **254,** 14–24
17. Cole, A. R., Causeret, F., Yadirgi, G., Hastie, C. J., McLauchlan, H., McManus, E. J., Hernandez, F., Eickholt, B. J., Nikolic, M., and Sutherland, C. (2006) *J. Biol. Chem.* **281,** 16591–16598
18. Lee, S., Kim, J. H., Lee, C. S., Kim, Y., Heo, K., Ihara, Y., Goshima, Y., Suh, P. G., and Ryu, S. H. (2002) *J. Biol. Chem.* **277,** 6542–6549
19. Dasgupta, B., and Gutmann, D. H. (2003) *Curr. Opin. Genet. Dev.* **13,** 20–27
20. Fahsold, R., Hoffmeyer, S., Mischung, C., Gille, C., Ehlers, C., Kucukceylan, N., Abdel-Nour, M., Gewies, A., Peters, H., Kaufmann, D., Buske, A., Tinschert, S., and Nurnberg, P. (2000) *Am. J. Hum. Genet.* **66,** 790–818
21. Minturn, J. E., Geschwind, D. H., Fryer, H. J., and Hockfield, S. (1995) *J. Comp. Neurol.* **355,** 369–379
22. Hamajima, N., Matsuda, K., Sakata, S., Tamaki, N., Sasaki, M., and Nonaka, M. (1996) *Gene (Amst.)* **180,** 157–163
23. Ozon, S., Byk, T., and Sobel, A. (1998) *J. Neurochem.* **70,** 2386–2396
24. Wang, L. H., and Strittmatter, S. M. (1996) *J. Neurosci.* **16,** 6197–6207
25. Goshima, Y., Nakamura, F., Strittmatter, P., and Strittmatter, S. M. (1995) *Nature* **376,** 509–514
26. Hedgecock, E. M., Culotti, J. G., Thomson, J. N., and Perkins, L. A. (1985) *Dev. Biol.* **111,** 158–170
27. Hedgecock, E. M., Culotti, J. G., Hall, D. H., and Stern, B. D. (1987) *Development (Camb.)* **100,** 365–382
28. Desai, C., Garriga, G., McIntire, S. L., and Horvitz, H. R. (1988) *Nature* **336,** 638–646
29. Kimura, T., Watanabe, H., Iwamatsu, A., and Kaibuchi, K. (2005) *J. Neurochem.* **93,** 1371–1382
30. Uchida, Y., Ohshima, T., Sasaki, Y., Suzuki, H., Yanai, S., Yamashita, N., Nakamura, F., Takei, K., Ihara, Y., Mikoshiba, K., Kolattukudy, P., Honnorat, J., and Goshima, Y. (2005) *Genes Cells* **10,** 165–179
31. Sayas, C. L., Moreno-Flores, M. T., Avila, J., and Wandosell, F. (1999) *J. Biol. Chem.* **274,** 37046–37052
32. Luo, L. (2000) *Nat. Rev. Neurosci.* **1,** 173–180
33. Hirose, M., Ishizaki, T., Watanabe, N., Uehata, M., Kranenburg, O., Moolenaar, W. H., Matsumura, F., Maekawa, M., Bito, H., and Narumiya, S. (1998) *J. Cell Biol.* **141,** 1625–1636
34. Bito, H., Furuyashiki, T., Ishihara, H., Shibasaki, Y., Ohashi, K., Mizuno, K., Maekawa, M., Ishizaki, T., and Narumiya, S. (2000) *Neuron* **26,** 431–441
35. Nakayama, A. Y., Harms, M. B., and Luo, L. (2000) *J. Neurosci.* **20,** 5329–5338
36. Lew, J., Huang, Q. Q., Qi, Z., Winkfein, R. J., Aebersold, R., Hunt, T., and Wang, J. H. (1994) *Nature* **371,** 423–426
37. Nikolic, M., Dudek, H., Kwon, Y. T., Ramos, Y. F., and Tsai, L. H. (1996) *Genes Dev.* **10,** 816–825
38. Chae, T., Kwon, Y. T., Bronson, R., Dikkes, P., Li, E., and Tsai, L. H. (1997) *Neuron* **18,** 29–42
39. Nikolic, M., Chou, M. M., Lu, W., Mayer, B. J., and Tsai, L. H. (1998) *Nature* **395,** 194–198
40. Owen, R., and Gordon-Weeks, P. R. (2003) *Mol. Cell. Neurosci.* **23,** 626–637
41. Cole, A., Frame, S., and Cohen, P. (2004) *Biochem. J.* **377,** 249–255
42. Yoshimura, T., Arimura, N., Kawano, Y., Kawabata, S., Wang, S., and Kaibuchi, K. (2006) *Biochem. Biophys. Res. Commun.* **340,** 62–68

Supplemental Material can be found at:
http://www.mcponline.org/cgi/content/full/M900179-MCP200
/DC2

An Integrated Approach of Differential Mass Spectrometry and Gene Ontology Analysis Identified Novel Proteins Regulating Neuronal Differentiation and Survival*[S]

Daiki Kobayashi‡, Jiro Kumagai§, Takashi Morikawa‡, Masayo Wilson-Morifuji‡, Anthony Wilson‡, Atsushi Irie¶, and Norie Araki‡‖

MS-based quantitative proteomics is widely used for large scale identification of proteins. However, an integrated approach that offers comprehensive proteome coverage, a tool for the quick categorization of the identified proteins, and a standardized biological study method is needed for helping the researcher focus on investigating the proteins with biologically important functions. In this study, we utilized isobaric tagging for relative and absolute quantification (iTRAQ)-based quantitative differential LC/MS/MS, functional annotation with a proprietary gene ontology tool (Molecular Annotation by Gene Ontology (MANGO)), and standard biochemical methods to identify proteins related to neuronal differentiation in nerve growth factor-treated rat pheochromocytoma (PC12) cells, which serve as a representative model system for studying neuronal biological processes. We performed MS analysis by using both nano-LC-MALDI-MS/MS and nano-LC-ESI-MS/MS for maximal proteome coverage. Of 1,482 non-redundant proteins semiquantitatively identified, 72 were differentially expressed with 39 up- and 33 down-regulated, including 64 novel nerve growth factor-responsive PC12 proteins. Gene ontology analysis of the differentially expressed proteins by MANGO indicated with statistical significance that the up-regulated proteins were mostly related to the biological processes of cell morphogenesis, apoptosis/survival, and cell differentiation. Some of the up-regulated proteins of unknown function, such as PAIRBP1, translationally controlled tumor protein, prothymosin α, and MAGED1, were further analyzed to validate their significant functions in neuronal differentiation by immunoblotting and immunocytochemistry using each antibody combined with a specific short interfering RNA technique. Knockdown of these proteins caused abnormal cell morphological changes, inhibition of neurite formation, and cell death during each course of the differentiation, confirming their important roles in neurite formation and survival of PC12 cells. These results show that our iTRAQ-MANGO-biological analysis framework, which integrates a number of standard proteomics strategies, is effective for targeting and elucidating the functions of proteins involved in the cellular biological process being studied. ***Molecular & Cellular Proteomics 8:2350–2367, 2009.***

MS-based quantitative proteomics strategies such as iTRAQ[1] (1) and stable isotope labeling with amino acids in cell culture (2) are powerfully effective for the comprehensive characterization of biological phenomena (1–5). Although these methods have been applied for cancer biomarker (6, 7) and drug target (8) discovery, their use in the elucidation of biological and functional processes has been limited because of certain technical problems that arise when attempting to meaningfully process the immense amount of data obtained from such experiments. The following four main issues are typically the sources of such difficulties. 1) Quantitative identification by one type of MS system may fail to cover the total proteome because of ionization efficiency differences, such as those between ESI and MALDI, for certain peptides, leading to theoretical limitations in proteome coverage. 2) The public protein databases are often insufficient for searching non-human species because of the limited available genomic information. 3) The identification of the functions and biological processes of thousands of proteins is a formidable task because of the lack of simple and user-friendly software to automate gene ontology (GO) annotation. Furthermore it is

From the Departments of ‡Tumor Genetics and Biology and ¶Immunogenetics, Graduate School of Medical Sciences, Kumamoto University and §General Research Core Laboratory, Kumamoto University Medical School, 1-1-1 Honjo, Kumamoto 860-8556, Japan

Received, April 7, 2009, and in revised form, June 12, 2009
Published, MCP Papers in Press, June 13, 2009, DOI 10.1074/mcp.M900179-MCP200

[1] The abbreviations used are: iTRAQ, isobaric tagging for relative and absolute quantitation; NGF, nerve growth factor; GO, gene ontology; PC12PRS, PC12 proteome reference set; ICC, immunocytochemistry; siRNA, short interfering RNA; TCTP, translationally controlled tumor protein; ProTα, prothymosin α; TrkA, tropomyosin-related kinase A; 2-D, two-dimensional; RP, reverse phase; GOA, gene ontology annotation; PCNA, proliferating cell nuclear antigen; PI, propidium iodide; PAIRBP1, plasminogen activator inhibitor 1 RNA-binding protein; PAI, plasminogen activator inhibitor; mESC, mouse embryonic stem cell; MAGE, melanoma antigen; p75NTR, p75 neurotrophin receptor; QqTOF, quadrupole/quadrupole/time-of-flight mass spectrometers.

difficult to convert large lists of taxonomically diverse proteins into their human orthologs to obtain the richest GO information available. 4) Lastly biological validation strategies for identified proteins have not been standardized. Therefore, we believe an analysis framework that provides (*a*) comprehensive proteome data; (*b*) a simple and quick tool for organizing, enriching, and sorting those data to reveal candidate molecules for relation to certain processes; and (*c*) a standardized biological validation technique would greatly benefit this field. We therefore designed a concise, three-step, sequential proteomics strategy that addresses the above concerns and utilized it successfully in studying the mechanism of neuronal differentiation in PC12 cells.

PC12 cells (9) have been widely used as a model of neurons because of their unique advantages, such as stability, homogeneity, strong nerve growth factor (NGF) responsiveness, high differentiation potential, and a wealth of accessible background material, which help to facilitate their manipulation (10). This cell line has also been used for studying the mechanisms of neuronal disorders such as Alzheimer (11), Huntington (12), and Parkinson diseases (13) and neurofibromatosis type 1 (14–16). Here we used PC12 cells as a model for characterizing the mechanisms of neuronal differentiation and neurodegenerative disorders by means of MS-based quantitative proteomics.

NGF is one member of a family of structurally and functionally related dimeric polypeptides, neurotrophins, that are essential for the development and maintenance of distinct neuronal populations in the central and peripheral nervous systems (17). The initial signaling cascades in the neuronal cells right after NGF stimulation have been subjected to thorough investigation and characterization by using PC12 cells. After binding of extracellular NGF to the cell membrane-localized tropomyosin-related kinase A (TrkA) receptor, TrkA receptors dimerize and subsequently autophosphorylate each other. Then the phosphorylated receptors recruit a complex of signaling molecules and induce a number of intracellular signaling cascades involving the signaling molecules, such as phosphoinositide 3-kinase, phospholipase C-γ, and Ras (18). The posttranslational modifications, such as phosphorylation cascades, triggered by NGF stimulation play important roles in PC12 cell differentiation. However, knowledge of the precise dynamic molecular events of protein expression in response to NGF signaling in PC12 cells after an interval that allows the stimulation to take full effect and produce morphological changes remains far from complete.

Several reported studies have applied such methods as expressed sequence tag (19), restriction landmark cDNA scanning (20), targeted display (21), serial analysis of gene expression (22), and cDNA microarray (23) to survey the global change of differentially expressed genes in PC12 cells before and after NGF treatment (19–23). However, the genes and underlying mechanisms associated with the acquisition of a neuronal phenotype in these cells have not been clarified. Also a few proteomics approaches have been used for identifying the proteins related to NGF-inducible neurite formation in PC12 cells. For example, 2-D electrophoresis was applied in whole-cell extract separation to study the NGF modulation of protein synthesis (24); however, only two peptides were identified (25). Even currently available PC12 cell 2-D databases include merely a few proteins related to NGF stimulation (26–29). There is thus a paucity of functional proteomic information related to PC12 cell biological processes that may be attributed to technical limitations such as those listed above.

In this study, we performed the first proteomics survey of proteins differentially expressed in PC12 cells during NGF treatment by using a semiquantitative differential LC shotgun method, namely isobaric tagging for relative and absolute quantitation (iTRAQ) coupled with concurrent use of two tandem MS/MS systems, namely nano-LC-MALDI-TOF-TOF and nano-LC-ESI-Quadrupole/quadrupole/time-of-flight mass spectrometers. The total list of proteins identified was converted into a new file linked to the GO database by our proprietary GO analysis tool for proteomes (MANGO) and categorized by biological process and function using specific classification methods. Thereafter we classified the subset of proteins that were up- or down-regulated during neurite formation into specific molecular categories by combining the differential data obtained by iTRAQ with the proteomic GO analysis results. We then attempted to characterize the functional mechanism of NGF-induced PC12 cell neuronal differentiation. Interestingly the specific up-regulated groups classified in this study were related to apoptosis/cell survival in addition to cell motility, differentiation, stress stimulation, and morphogenesis. To investigate the molecular functions of the up-regulated proteins in relation to both PC12 cell differentiation and apoptosis/survival during neurite formation, some of them were further analyzed with a biochemical and cellular biological strategy using a combined antibody and siRNA technique. Lastly we demonstrated the advantages that our concise, sequential proteomics strategy offers for studying the molecular mechanisms of cellular biological events such as cell differentiation and survival/apoptosis.

EXPERIMENTAL PROCEDURES

Cell Culture, NGF Treatment, and Preparation of Cell Lysate—PC12 cells were cultured under 5% CO_2 at 37 °C in Dulbecco's modified Eagle's medium supplemented with 10% horse serum and 5% fetal bovine serum. We performed four independent cell cultures for a fourplex iTRAQ analysis. Two of them were used as duplicated samples for controls, and the other two samples were used as NGF-treated cells. For NGF stimulation, the cells were cultured onto collagen-coated culture dishes (Iwaki) in the same medium and stimulated with 50 ng/ml 2.5 S NGF (Wako) at 48 h. For preparation of cell lysate, cells were solubilized with the lysis buffer containing 8 M urea, 2% CHAPS, 2 mM Na_2VO_4, 10 mM NaF, 1 μM okadaic acid, and 1% (v/v) protease inhibitor mixture (Sigma) and passed through a 25-gauge syringe 15 times. Lysates were centrifuged at 13,000 × *g* for 20 min at 4 °C, and the protein concentration of the supernatants was determined using the Bio-Rad protein assay.

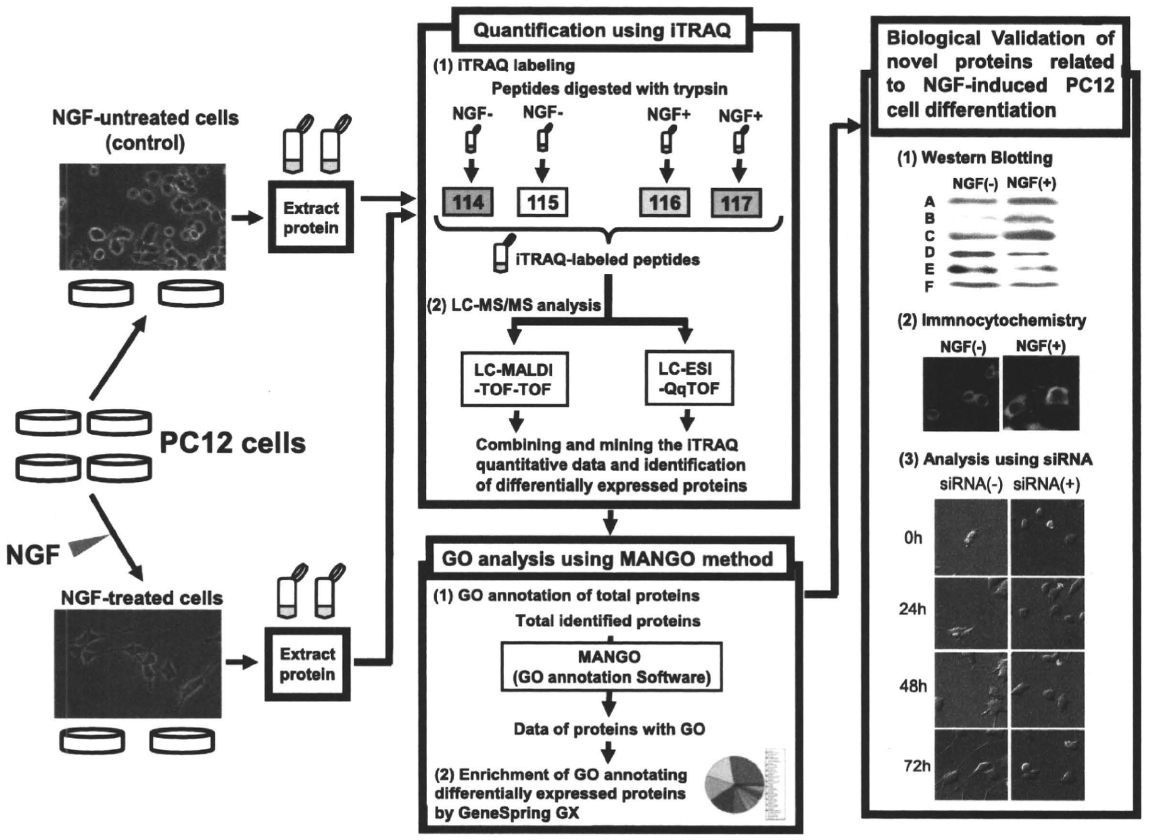

FIG. 1. **Work flow for the identification of the novel proteins regulating NGF-induced differentiation in PC12 cells.** For the fourplex iTRAQ labeling, the four lysates of PC12 cells separately cultured were prepared in parallel. The tryptic peptides from untreated cells and NGF-treated cells were labeled using mass 114/115 and 116/117 isobaric iTRAQ tags, respectively. These labeled peptides were analyzed with LC-MALDI-TOF-TOF or LC-ESI-QqTOF, and the quantification of each protein was performed according to the obtained iTRAQ data. Further biological and functional interpretation of the differentially expressed proteins was carried out by proteomics GO analysis using the MANGO method followed by cell biological analyses. Proteins *A–F* are candidates for novel molecules related to NGF-induced PC12 cell differentiation.

iTRAQ Sample Labeling—One hundred micrograms of each protein sample was precipitated using a 2-D Clean-Up kit (Amersham Biosciences), and the precipitants were dissolved in 10 μl of 6 M urea. iTRAQ sample labeling was performed according to the manufacturer's protocol with minimum modification. For the fourplex iTRAQ labeling, the four lysates of PC12 cells separately cultured were treated with iTRAQ reagents in parallel. Twenty microliters of dissolution buffer and 1 μl of denaturant reagent were added to the samples. The samples were reduced by addition of 2 μl of reducing reagent and incubation at 60 °C for 1 h. Reduced cysteine residues were then blocked by addition of 1 μl of cysteine blocking reagent and incubated at room temperature for a further 10 min. Tryptic digestion was initiated by the addition of 12.5 μl of trypsin solution (Promega; prepared as 1 μg/μl in water solution) and incubated at 37 °C for 16 h. To label the peptides with iTRAQ reagents, one vial of labeling reagent was thawed and reconstituted in 80 μl of ethanol. The reagents 114 and 115 for two samples from untreated cells and the reagents 116 and 117 for two samples from NGF-stimulated cells were added to the digests and incubated for 1 h at room temperature. The labeled samples were then mixed together before fractionation using a cation exchange column.

Sample Fractionation and Desalting—To remove excess, unbound iTRAQ reagent and to simplify the peptide mixture, the labeled peptide mixture was purified and fractionated using a GE Healthcare AKTA system. The mixed sample was diluted in loading buffer (20% (v/v) ACN and 10 mM potassium phosphate, pH 3.0) and loaded onto a Mono S column (GE Healthcare) equilibrated with loading buffer. Peptides were eluted with a gradient of solvent B (10 mM potassium phosphate, pH 3.0, and 1 M KCl in 20% (v/v) ACN) as follows: 0–2 min, 0–7% B; at 6 min, to 14% B; at 8 min, to 32% B; at 13 min, to 70% B; and at 21 min, to 100% B. Twenty-five fractions that included the iTRAQ-labeled peptides were used for analysis. The fractions were dried in a vacuum centrifuge and rehydrated with solution containing 2% ACN and 0.1% TFA. The samples were desalted with ZipTip^{TM} μ-C_{18} pipette tips (Millipore). The desalted peptides were divided into two fractions to analyze the same samples by using nano-LC-MALDI-TOF-TOF and nano-LC-ESI-QqTOF systems.

LC-MALDI-MS/MS Analysis—Samples were separated by C_{18} nano-LC using DiNa Map (KYA Tech Corp.) equipped with a device spotting eluted fractions on a MALDI plate. Sample was injected onto a C_{18} column (0.5-mm inner diameter × 1-mm length, KYA Tech Corp.) equilibrated with solvent A (2% ACN and 0.1% TFA) and resolved on a C_{18} nanocolumn (0.15-mm inner diameter × 100-mm length; KYA Tech Corp.) at a flow rate of 300 nl/min with a 90-min gradient of solvent B (70% ACN and 0.1% TFA) as follows: 0–20% B from 0 to 10 min, to 50% B at 65 min, and to 100% B at 75 min. Column effluent was mixed with matrix (2 mg/ml α-cyano-4-hydroxycinnamic acid in 50% ACN and 0.1% TFA) at a flow rate of 1.4 μl/min.

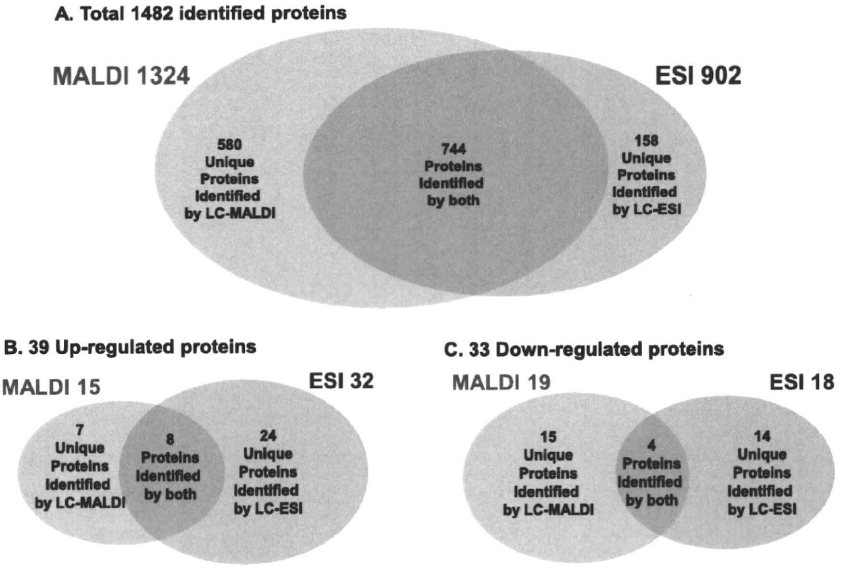

FIG. 2. **Venn diagrams of the number of total (*A*), up-regulated (*B*), and down-regulated (*C*) proteins identified by iTRAQ.** *A*, in total, 1,482 proteins of all taxonomies listed in supplemental Table 1 were identified with a confidence limit of 95%. *B* and *C*, for quantification of each protein identified by MALDI or ESI, a -fold change of each protein expression was calculated by comparing the average iTRAQ ratio of 116 and 117 as NGF-treated groups with the average ratio of 114 and 115 as control groups. Proteins quantified with a -fold change more than 20% (average iTRAQ ratio >1.20 or <0.83) and a p value less than 0.05 by MALDI or ESI were identified as differentially expressed proteins (*B* and *C*).

Fractions were spotted at 30-s intervals onto a stainless steel MALDI target plate (192 wells/plate; Applied Biosystems). Mass spectra of the peptides were acquired on a 4700 Proteomics Analyzer (Applied Biosystems) using 4000 Series Explorer software (Version 3.6). Mass spectra from m/z 800 to 4,000 were acquired for each fraction with 1,500 laser shots. To analyze the less abundant peptides, all of the peaks with a signal to noise ratio threshold from 50 to 75 and from 75 to 100 in each MS spectrum were selected for MS/MS analysis with 5,000 and 4,000 laser shots, respectively. Next all of the peaks above a signal to noise ratio threshold of 100 were selected for MS/MS analysis with 3,000 laser shots. Fragmentation of the labeled peptides was induced by the use of atmosphere as a collision gas with a pressure of 1×10^{-6} Torr and a collision energy of 1 kV.

LC-ESI-MS/MS Analysis—Samples were analyzed by nano-LC-ESI-MS/MS using the LC Packings Ultimate instrument fitted with a 20-μl sample loop. Samples were loaded onto a 5-mm RP C_{18} precolumn (LC Packings) at 30 μl/min and washed for 10 min before switching the precolumn in line with the separation column. The separation column used was a 75-μm internal diameter $\times$ 150-mm length PepMap RP column from LC Packings packed with 3-μm C_{18} beads with 100-Å pores. The flow rate used for separation on the RP column was 200 nl/min with a 90-min gradient of solvent B (85% ACN and 0.1% formic acid) as follows: 0–40% B from 0–60 min to 100% B at 70 min. The samples were divided into two fractions beforehand, and the first analysis was performed on a QSTAR Pulsar i mass spectrometer (Applied Biosystems/MDS Sciex), and the software used for data acquisition was Analyst QS 1.1 (Applied Biosystems/MDS Sciex) with the scan cycles set up to perform a 1-s MS scan followed by three MS/MS scans of the three most abundant peaks for 3 s each. Data acquisition was performed with an exclusion of 60 s for previous target ions. To analyze the less abundant peptides, the second analysis was performed under the same condition except for input of the m/z list to exclude the analyses of peptide ions already analyzed in the first run. The labeled peptides were fragmented under CID conditions designed to give iTRAQ reporter ions.

Data Analysis—Data from MALDI or ESI analysis were analyzed using the Paragon™ algorithm (30) of ProteinPilot Version 2.0 (Applied Biosystems), and the database searched was the Swiss-Prot database with all taxonomy (Revision number 53, 269,293 sequence entries, updated on May 29, 2007). Identified proteins were grouped by the Paragon algorithm of the software to minimize redundancy. This software has a function of automatic grouping of identified proteins according to the identified peptide sequence. The identified proteins were automatically grouping by the Paragon algorithm. Peptides used for the quantification of proteins were chosen by this algorithm of ProteinPilot software. All peptides used for the calculation of protein ratios were unique to the given protein or proteins within the group; peptides that were common to other isoforms or proteins of the same family that were reported separately were ignored. The ProteinPilot cutoff score used was 1.3, which corresponds to a confidence limit of 95%. The six user-defined options used included (i) cysteine alkylation, methyl methane thiosulfate; (ii) digestion, trypsin digestion; (iii) special factors, none; (iv) species, all species; (v) identification focus, biological modifications; and (vi) search effort, thorough identification search. For quantification of each protein identified in the MALDI or ESI analysis, a -fold change of each protein expression was calculated by comparing the average iTRAQ ratio of 116 and 117 as NGF-treated groups with the average ratio of 114 and 115 as control groups. Proteins quantified with a -fold change of more than 20% (average iTRAQ ratio >1.20 or <0.83) and a p value less than 0.05 (Student's t test) in the MALDI or ESI analysis were identified as differentially expressed proteins.

Proteomics GO Analysis by MANGO Method—To automate both the conversion of all identified proteins of multiple taxonomies into their human orthologs and annotation with GO information, a tool for taxonomy conversion/GO annotation, Molecular Annotation by Gene Ontology (MANGO), was designed as a Web-based application using the mySQL 4.0 database management system and scripts written in Java. Ensembl Mart and UniProt GOA (GOA UniProt Version 49.0, June 2007 update) files were integrated into the database and were used as the external reference data for the taxonomy conversion and the GO annotation, respectively. For the proteins that could not be automatically converted to the human orthologs using this conversion/annotation tool, we searched the human orthologs by using National Center for Biotechnology Information basic local alignment search tool (NCBI BLAST) programs. A list of 1,404 human GO-annotated proteins was compiled and was designated as the PC12 proteome reference set for analysis with GeneSpring GX (supplemental Table 4). GeneSpring GX Version 7.3.1 was used to determine the GO categories that were statistically overrepresented in the iTRAQ data set. GO categories, by which at least three proteins were annotated, were accepted at the significance level of $p < 0.05$ (Fisher's

TABLE I

List of proteins differentially-expressed in response to NGF stimulation

snRNA, small nuclear RNA; —, not applicable.

Protein name abbreviation	Protein name	Accession no.	Theoretical molecular mass (kDa)/pI	MALDI		ESI		Ref.[b]
				Average ratio[a]	*p* value	Average ratio[a]	*p* value	
Up-regulated proteins								
VGF	Neurosecretory protein VGF	P20156	68.2/4.7	**2.935**	0.011	**3.770**	0.024	23, 40
NEUM	Neuromodulin	P07936	23.6/4.6	**1.791**	0.008	**2.936**	0.021	23, 41
MOES	Moesin	O35763	67.7/6.2	**1.691**	0.035	**1.679**	0.030	—
CMGA	Chromogranin A	P10354	52.0/4.7	**1.594**	0.003	**1.596**	0.003	42
ANXA2	Annexin A2	Q07936	38.7/7.6	**1.449**	0.048	**1.805**	0.037	23, 43
PERI	Peripherin	P21807	53.5/5.4	**1.329**	0.011	**1.429**	0.012	44
AT1A1	Sodium/potassium-transporting ATPase α-1 chain	P06685	11.3/5.3	**1.271**	0.048	**1.341**	0.003	23
MAP1B	Microtubule-associated protein 1B	P15205	269.5/4.7	**1.250**	0.010	**1.352**	0.027	45
SQSTM	Sequestosome-1	O08623	47.7/5.1	**1.764**	0.042			—
RIR2	Ribonucleoside-diphosphate reductase M2 subunit	Q4KLN6	45.0/5.5	**1.339**	0.044			—
SGTA	Small glutamine-rich tetratricopeptide repeat-containing protein A	O70593	34.2/5.1	**1.286**	0.035	1.051	0.787	—
CROP	Cisplatin resistance-associated overexpressed protein	O95232[c]	51.5/9.8	**1.266**	0.042	1.006	0.294	—
PAIRBP1	Plasminogen activator inhibitor 1 RNA-binding protein	Q6AXS5	44.8/8.6	**1.226**	0.013	1.241	0.113	—
GSPT1	G_1 to S phase transition protein 1 homolog	P15170[c]	55.8/5.5	**1.206**	0.042	0.977	0.841	—
CRIP2	Cysteine-rich protein 2	P36201	22.7/8.9	**1.205**	0.020			—
PROTA	Prothymosin α	P06302	12.4/3.8	1.642	0.206	**2.173**	0.037	—
AHNAK	Neuroblast differentiation-associated protein AHNAK	Q09666[c]	629.1/5.8	1.245	0.113	**1.947**	0.012	46
SCG2	Secretogranin-2	P10362	71.0/4.7	1.339	0.068	**1.633**	0.027	42
AT1B1	Sodium/potassium-transporting ATPase subunit β-1	P07340	35.2/8.8	1.423	0.062	**1.630**	0.001	23
MAGED1	Melanoma-associated antigen D1	Q9ES73	85.8/7.1	1.066	0.654	**1.630**	0.020	—
LEG1	Galectin-1	P11762	14.9/5.1	1.272	0.126	**1.578**	0.016	22, 23
ENPL	Endoplasmin	P14625[c]	92.5/4.8	1.052	0.134	**1.556**	0.016	22, 23
S100A6	Protein S100-A6	P05964	10.0/5.3	1.362	0.069	**1.552**	0.004	—
E2IG5	E2-induced gene 5 protein homolog	Q4QQV3	17.8/10.0	1.240	0.103	**1.547**	0.023	23
CRMP4	Dihydropyrimidinase-related protein 3 (CRMP4)	Q62952	62.0/6.0	1.183	0.240	**1.407**	0.016	23
SRRM2	Serine/arginine repetitive matrix protein 2	Q8BTI8[d]	294.7/12.0	0.981	0.667	**1.377**	0.013	—
DNJA1	DnaJ homolog subfamily A member 1	P63036	44.9/6.7	1.065	0.397	**1.331**	0.011	—
RAC1	Ras-related C3 botulinum toxin substrate 1	Q6RUV5	21.5/8.8			**1.316**	0.044	—
TCTP	Translationally controlled tumor protein	P63029	19.5/4.8	1.359	0.126	**1.291**	0.016	—
RAB2A	Ras-related protein Rab-2A	P05712	23.5/6.1	1.272	0.239	**1.280**	0.015	—
OXRP	Hypoxia up-regulated protein 1	Q63617	111.3/5.1	1.051	0.591	**1.271**	0.008	—
PRDX6	Peroxiredoxin-6	O35244	24.8/5.6	1.128	0.207	**1.268**	0.008	—
ENOA	α-Enolase	P04764	47.1/6.2	1.153	0.172	**1.253**	0.008	23
RADI	Radixin	P35241[c]	68.6/6.0	0.885	0.193	**1.251**	0.032	23
ALDR	Aldose reductase	P07943	35.8/6.3	1.276	0.235	**1.248**	0.004	—
PDI	Protein-disulfide isomerase	P04785	57.0/4.8	1.041	0.118	**1.245**	0.045	23
FABPE	Fatty acid-binding protein, epidermal	P55053	15.1/6.73	1.136	0.268	**1.227**	0.049	23
RGP1	Ran GTPase-activating protein 1	P46061[d]	63.6/4.6	1.027	0.359	**1.219**	0.012	—
NUCB1	Nucleobindin-1	Q63083	53.5/5.0	1.039	0.521	**1.208**	0.005	—
Down-regulated proteins								
K1C18	Keratin, type I cytoskeletal 18	Q5BJY9	47.8/5.2	**0.626**	0.028	**0.566**	0.043	—
K2C8	Keratin, type II cytoskeletal 8	Q10758	54.0/5.8	**0.690**	0.011	**0.599**	0.040	—
PRPS2	Ribose-phosphate pyrophosphokinase II	P09330	34.8/6.2	**0.690**	0.040	**0.642**	0.015	—
LDHA	L-Lactate dehydrogenase A chain	P04642	36.5/8.5	**0.768**	0.022	**0.792**	0.041	—
PRP19	Pre-mRNA-processing factor 19	Q9JMJ4	55.2/6.2	**0.551**	0.009	0.880	0.604	—
VTDB	Vitamin D-binding protein	P04276	53.5/5.7	**0.625**	0.006			—
IDHP	Isocitrate dehydrogenase (NADP), mitochondrial	P56574	51.0/8.9	**0.630**	0.005	0.868	0.068	—
HNRLL	Heterogeneous nuclear ribonucleoprotein L-like	Q921F4[d]	64.1/5.8	**0.651**	0.031	0.636	0.187	—
NUCKS	Nuclear ubiquitous casein and cyclin-dependent kinase substrate	Q9EPJ0	27.1/5.0	**0.747**	0.006			—
API5	Apoptosis inhibitor 5	Q9BZZ5[c]	57.6/5.8	**0.748**	0.013	0.777	0.116	—
H2B1C	Histone H2B type 1	Q00715	14.0/10.4	**0.762**	0.040	0.860	0.003	23
RL34	60 S ribosomal protein L34	P11250	13.5/11.7	**0.769**	0.049			—
RLA0	60 S acidic ribosomal protein P0	P19945	34.2/5.9	**0.772**	0.035	0.962	0.605	—
TBB4	Tubulin β-4 chain	P04350[c]	49.6/4.8	**0.784**	0.034			—
SRR35	35-kDa SR repressor protein	Q8WXF0[c]	30.5/11.7	**0.787**	0.001			—
PCNA	Proliferating cell nuclear antigen	P04961	28.7/4.6	**0.790**	0.043	0.743	0.060	—

TABLE I—*continued*

Protein name abbreviation	Protein name	Accession no.	Theoretical molecular mass (kDa)/pI	MALDI		ESI		Ref.[b]
				Average ratio[a]	*p* value	Average ratio[a]	*p* value	
UBP48	Ubiquitin carboxyl-terminal hydrolase 48	Q76LT8	118.8/5.9	**0.793**	0.016			—
GSTM2	Glutathione *S*-transferase Mu 2	P08010	25.7/6.9	**0.794**	0.024	0.825	0.055	23
CB39L	Calcium-binding protein 39-like	Q9H9S4[c]	39.1/8.5	**0.818**	0.033			—
LSM8	U6 snRNA-associated Sm-like protein LSm8	O95777[c]	10.4/4.4			**0.648**	0.015	—
DDC	Aromatic-L-amino-acid decarboxylase	P14173	54.1/6.5			**0.669**	0.045	23
CSK21	Casein kinase II subunit α	P19139	45.1/7.3	0.875	0.088	**0.670**	0.041	—
RL6	60 S ribosomal protein L6	P21533	33.6/10.7	0.904	0.497	**0.681**	0.040	—
GALK1	Galactokinase	Q9R0N0[d]	42.2/5.2	1.222	0.509	**0.730**	0.029	—
AB14B	Abhydrolase domain-containing protein 14B	Q8VCR7[d]	22.5/5.8	0.675	0.292	**0.748**	0.030	—
HNRPF	Heterogeneous nuclear ribonucleoprotein F	Q794E4	45.7/5.3	1.053	0.294	**0.756**	0.031	—
APT	Adenine phosphoribosyltransferase	P36972	19.5/6.2	0.942	0.724	**0.783**	0.028	—
H2A2B	Histone H2A type 2-B	Q8IUE6[c]	14.0/10.9	0.860	0.157	**0.814**	0.024	23
FUBP2	Far upstream element-binding protein 2	Q99PF5	74.2/6.4	0.949	0.090	**0.818**	0.002	—
FINC	Fibronectin	P04937	272.5/5.5	0.688	0.172	**0.819**	0.000	—
TIM13	Mitochondrial import inner membrane translocase subunit Tim13	P62076	10.5/8.4	1.003	0.974	**0.820**	0.025	—
SFRS2	Splicing factor, arginine/serine-rich 2	Q6PDU1	25.5/11.9	0.852	0.249	**0.826**	0.005	—
FEN1	Flap endonuclease 1	P39748[c]	42.6/8.8	0.971	0.775	**0.833**	0.022	23

[a] The average ratio of iTRAQ data with *p* value smaller than 0.05 is highlighted with bold font.
[b] The proteins with Refs. 22 and 23 had been reported previously as NGF-responsive genes at the mRNA level.
[c] Proteins identified with human taxonomy.
[d] Proteins identified with mouse taxonomy.

exact test). The annotation data of the 72 differentially expressed proteins were used to determine the overrepresented biological processes related to NGF-induced PC12 cell differentiation. A GO tree view composed of enriched biological processes in the up-regulated proteins was built according to the tree view in AmiGO, a tool for searching and browsing the Gene Ontology database (31).

Western Blotting—Cell lysate samples containing 20 μg of total protein were electrophoresed on SDS-polyacrylamide gels, transferred onto a PVDF membrane by electroblotting, and subjected to immunoblotting with the indicated antibody. In the case of prothymosin α (Pro$T\alpha$), cell lysate samples were transferred onto a membrane by electroblotting with acidic buffer (20 mM sodium acetate buffer, pH 5.2) followed by fixation with 0.5% glutaraldehyde (32, 33). Membranes were probed with different primary antibodies followed by horseradish peroxidase-conjugated mouse, rabbit, and goat secondary antibodies (GE Healthcare). The images were visualized with ECL (GE Healthcare). The following primary antibodies were used: neurosecretory protein VGF, CRMP-4, galectin-1, Pro$T\alpha$, MAGED1, and PCNA (Santa Cruz Biotechnology); plasminogen activator inhibitor 1 RNA-binding protein (PAIRBP1) (Abnova Co.); translationally controlled tumor protein (TCTP) (MBL International Corp.); β-actin (Sigma); peroxiredoxin 6 (Lab Frontier); and protein-disulfide isomerase (Stressgen). For the quantitative analysis, the ECL patterns were scanned using LabScan 5.0 (GE Healthcare) with transparent mode and a resolution of 300 dpi. The intensities were measured using ProGenesis Workstation Version 2005 (PerkinElmer Life Sciences).

Transfection of PC12 Cells with siRNA—Transfection of PC12 cells with siRNA was performed using Lipofectamine 2000 (Invitrogen) according to the manufacturer's protocol. Four target sequences for rat, PAIRBP1, TCTP, Pro$T\alpha$, and MAGED1 siRNA, were designed as follows. A 21-oligonucleotide siRNA duplex was designed as recommended elsewhere and was synthesized by Gene Link to target the PAIRBP1 sequence (5′-^{1125}AAGUGCUUCUGCUCCUGACTT-3′), the TCTP sequence (5′-^{357}AAGCACATCCTTGCTAATTTT-3′), the Pro$T\alpha$ sequence (5′-52AAGGAGAAGAAGGAAGUUGTT-3′), and the MAGED1 sequence (5′-^{1928}AAGUGCUGAGAUUCAUUGCTT-3′). A Silencer Negative Control siRNA 1 (Ambion) was used as a control siRNA for the analysis.

Immunofluorescence Analysis—PC12 cells cultured on 35-mm collagen-coated culture dishes were fixed with 4% paraformaldehyde in PBS for 15 min at room temperature and then permeabilized with 0.1% Triton X-100 in PBS on ice for 15 min. After being washed with PBS, cells were incubated in primary antibodies diluted in PBS containing 5% bovine serum albumin followed by anti-mouse or -rabbit Alexa Fluor® 488-conjugated IgG (Invitrogen) for 60 min at room temperature. After being washed with PBS, the cells were incubated for 10 min at room temperature with rhodamine-phalloidin (Invitrogen) to stain cellular F-actin. After being washed with PBS, the cells were incubated for 10 min at room temperature with 20 μg/ml Hoechst33342 (Invitrogen) to stain nuclear actin. Analysis was performed with a fluorescence microscope (with 20 × 1.6 Olympus IX71) (DPController, DPManager).

Quantification of Neurite Outgrowth—For quantification of the neurite outgrowth of PC12 cells, the cells transfected with siRNAs were cultured onto collagen-coated culture dishes (Iwaki) under the condition of 1% horse serum and stimulated with 50 ng/ml 2.5 S NGF (Wako) at 48 h. Total neurite length of NGF-stimulated PC12 cells was measured using MetaMorph software (Molecular Devices). The total number of tip ends was manually counted to represent the number of neurites from individual cells. For each measurement, at least 50 cells per dish were analyzed from randomly selected fields. Each experiment was repeated three times.

Evaluation of PC12 Cell Death—Propidium iodide (PI) was used for the evaluation of PC12 cell death. Cells transfected with siRNAs were cultured onto 35-mm collagen-coated culture dishes (Iwaki) under the condition of 10% horse serum and 5% fetal bovine serum and stimulated with 50 ng/ml 2.5 S NGF (Wako) at 48 h. The cells were fixed with 4% paraformaldehyde in PBS and incubated with 0.2 μg/ml PI for apoptotic cells and 20 μg/ml Hoechst33342 (Invitrogen) for total cells for 10 min at room temperature. PI-positive cells were counted using a fluorescence microscope (with 20 × 1.6 Olympus IX71) (DPController, DPManager). For each counting, at least 500 cells per dish were counted from randomly selected fields. Each experiment was repeated three times.

Time Lapse Video Analysis—Cells were cultured on a collagen-coated glass bottom plate with 6 wells (Iwaki). The plate was main-

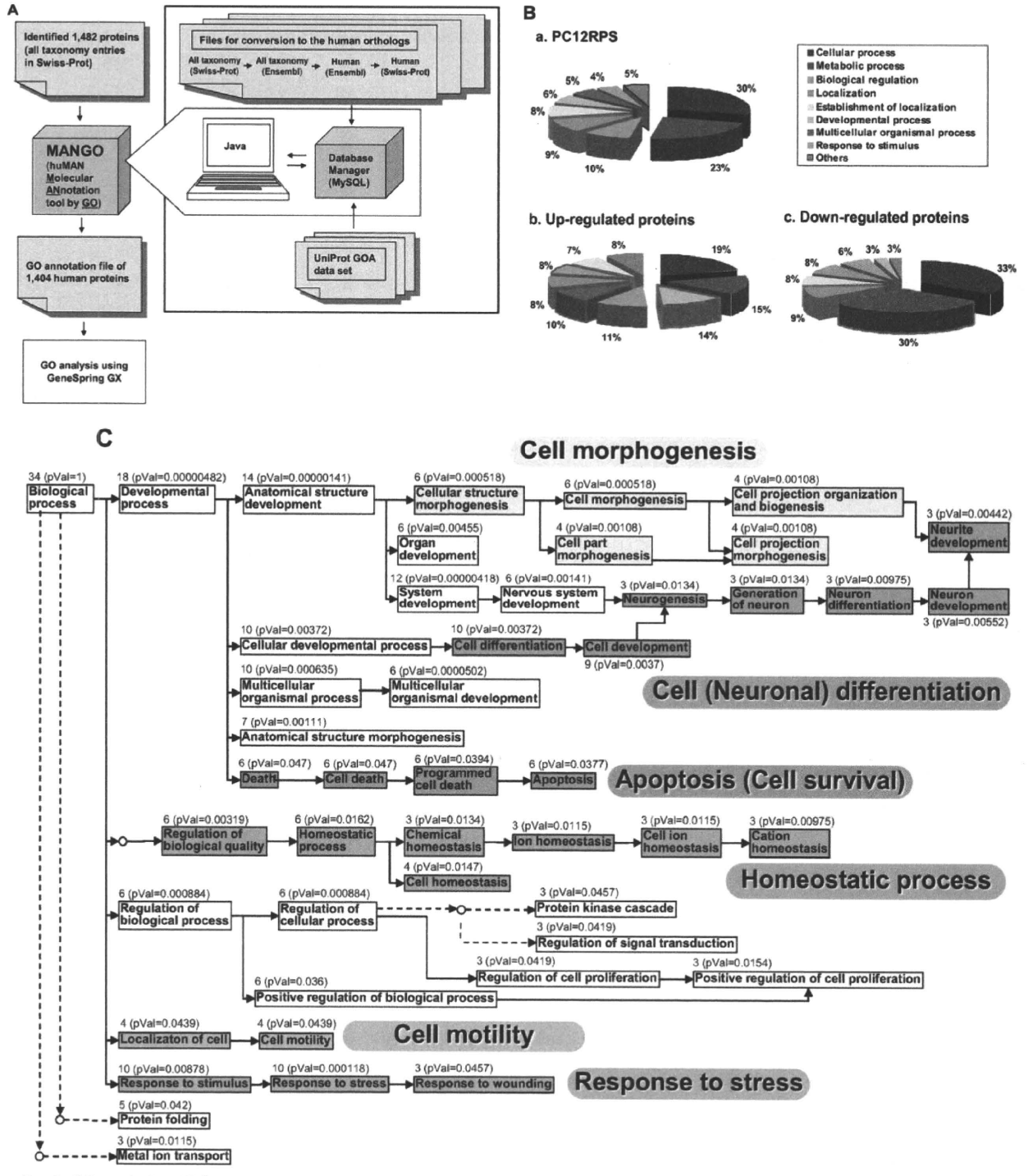

FIG. 3. **GO analysis of PC12 proteins differentially expressed after NGF stimulation.** *A*, work flow for proteomics GO analysis (MANGO method). MANGO (a Web application), composed of the mySQL 4.0 and scripts written in Java, automatically executed the following steps. First, 1,482 proteins with multiple species matches were converted to human orthologs according to the conversion steps using Ensembl Mart files shown in the figure. Then the converted human orthologs were annotated with GO according to the UniProt GOA data set (described under "Experimental Procedures"). The resulting list of 1,404 GO-annotated human proteins was used as the PC12PRS as shown in supplemental Table 4. GeneSpring GX was used to determine statistically overrepresented GO categories from the iTRAQ data set. *B*, classification by annotated biological processes of the PC12PRS (*a*), 39 up-regulated (*b*), and 33 down-regulated (*c*) proteins identified with the iTRAQ method.

tained at 37 °C under the air condition of 5% CO_2 in the chamber set under the camera during the observation. Images were obtained by using a 20× UPlan SApo objective (Olympus IX81). The camera, shutters, and filter wheel were controlled by MetaMorph imaging software (Molecular Devices), and the images were collected every 10 min with an exposure time of 50 ms.

RESULTS

Identification of Differentially Expressed Proteins in Response to NGF in PC12 Cells—For the fourplex iTRAQ labeling, four independent, separately cultured cell lysates were prepared in parallel. The tryptic peptides from untreated cells were labeled with mass 114 and 115 isobaric iTRAQ tags, and those from NGF-treated cells were labeled with mass 116 and 117 isobaric iTRAQ tags. The iTRAQ-labeled peptides were then fractionated by cation exchange column chromatography and analyzed with LC-MS/MS using both MALDI and ESI (Fig. 1).

With LC-MALDI-MS/MS, 1,324 proteins were identified from 14,710 peptide sequences; in contrast, with LC-ESI-MS/MS, 902 proteins were identified from 12,769 peptide sequences. Only 744 proteins were identified by both systems, and 580 and 158 proteins were uniquely identified with LC-MALDI-MS/MS and LC-ESI-MS/MS, respectively. In total, 1,482 proteins were identified with >95% confidence (Fig. 2*A* and supplemental Table 1). At a -fold change of >20% (ratio >1.20 or <0.83), 15 proteins identified with LC-MALDI-MS/MS were up-regulated, and 19 were down-regulated, whereas 32 identified with LC-ESI-MS/MS were up-regulated, and 18 were down-regulated (p value <0.05) (Fig. 2, *B* and *C*). Eight up- and four down-regulated proteins were identified by both systems, and seven or 24 up- and 15 or 14 down-regulated proteins were uniquely identified with LC-MALDI-MS/MS or LC-ESI-MS/MS, respectively (Fig. 2, *B* and *C*). In total, 72 proteins (39 up- and 33 down-regulated) were differentially expressed in response to NGF. Among the NGF-responsive proteins, 64 were newly identified in this study (Table I and supplemental Tables 2 and 3).

Proteomics GO Analysis of NGF-responsive Proteins—The list of differentially expressed proteins was prepared for use in GO analysis with GeneSpring using a new, in-house taxonomy conversion/GO annotation tool, MANGO (a Web application) (Fig. 3*A*). First the taxonomies of all 1,482 identified proteins (multiple species matches) were converted to the *Homo sapiens* taxonomy. 1,404 of them were assigned human orthologs and annotated with GO information from UniProt. This GO-annotated list, compiled using the MANGO tool, was designated as the PC12 proteome reference set (PC12PRS) on which two distinct proteomics GO analyses were subsequently performed (supplemental Table 4). In the first analysis, to determine the overrepresented biological processes specifically related to the NGF-induced PC12 cell differentiation, we simply compared the GO categories represented by the differentially expressed proteins in the PC12PRS with the GO categories represented by the PC12PRS overall (Fig. 3*B*). From this we found that the following biological processes occurred significantly more frequently in the GO annotations of the 39 up-regulated proteins than they did in the PC12PRS as a whole: "developmental process" (14 *versus* 6%), "multicellular organismal process" (10 *versus* 5%), and "response to stimulus" (8 *versus* 4%) (Fig. 3*B*, *a* and *b*). Also on the other hand, the occurrence ratio of "metabolic process" (30 *versus* 23%) was higher in the GO annotations of the 33 down-regulated proteins than in those of the PC12PRS as a whole (Fig. 3*B*, *a* and *c*). Next to obtain further statistical interpretation, a second proteomics GO analysis of the differentially expressed proteins in the PC12PRS (supplemental Table 4) was performed to determine which biological processes were enriched in the 39 up-regulated and the 33 down-regulated proteins (Table II). Using these data, a GO tree view was built to clarify the interrelationships of these biological processes (Fig. 3*C*). The part of the tree comprising the up-regulated proteins was mainly divided into six branches, which included "cell morphogenesis" (p value = 0.000518), "apoptosis (cell survival)" (p value = 0.0377), "homeostatic process" (p value = 0.0162), "cell motility" (p value = 0.000118), "response to stress" (p value = 0.000118), and "cell differentiation" (p value = 0.00372) (Tables II and III and Fig. 3*C*). On the other hand, the part of the tree comprising the down-regulated proteins included cellular metabolic processes, especially RNA and DNA metabolic processes (Tables II and III).

Biological Validation of Newly Identified NGF-responsive Proteins Related to GO Categories Extracted by MANGO—Of the six up-regulated groups listed in Table II, we focused on cell morphogenesis and apoptosis/cell survival (Fig. 3*C* and Table III) and used a time course analysis by Western blotting to study the expression patterns of the up-regulated proteins related to these processes (Fig. 4). Neurosecretory protein VGF, the most significantly up-regulated protein identified by both LC-MALDI-MS/MS and LC-ESI-MS/MS (Table I and supplemental Fig. 1), was used as a positive control of the time-dependently increased protein by Western blotting (Fig. 4). Seven proteins, CRMP-4, MAGED1, PAIRBP1, protein-disulfide isomerase, peroxiredoxin 6, ProTα, and TCTP, were up-regulated in response to NGF with different expression patterns in the time course study (Fig. 4, *A* and *B*, and supplemental Fig. 2). Interestingly TCTP and MAGED1 expression

C, a GO hierarchy tree of biological processes annotating the 39 up-regulated proteins. GO analysis was performed by using GeneSpring GX software. A GO tree view composed of enriched biological processes in the up-regulated proteins was built according to the tree view in AmiGO. Direct and indirect hierarchies are indicated by *full* and *dotted lines* with *arrows*, respectively. The number of molecules and p values (*pVal*) for biological processes annotated are shown in the tree.

TABLE II

Overrepresented biological processes by proteomics GO analysis of proteins differentially expressed in response to NGF stimulation

Categories	All proteins in category	Percentage of all proteins in category	Up- or down-regulated proteins in category	Percentage of up- or down-regulated proteins in category	*p* value
Up-regulated proteins					
GO:8150: biological process	1,245	100	34	100	1
GO:32502: developmental process	231	18.55	18	52.94	4.82e−06
GO:48856: anatomical structure development	126	10.12	14	41.18	1.41e−06
GO:32501: multicellular organismal process	186	14.94	13	38.24	0.000635
GO:48731: system development	99	7.952	12	35.29	4.18e−06
GO:7275: multicellular organismal development	125	10.04	12	35.29	5.02e−05
GO:6950: response to stress	95	7.631	10	29.41	0.000118
GO:48869: cellular developmental process	145	11.65	10	29.41	0.00372
GO:30154: cell differentiation	145	11.65	10	29.41	0.00372
GO:50896: response to stimulus	163	13.09	10	29.41	0.00878
GO:48468: cell development	121	9.719	9	26.47	0.0037
GO:9653: anatomical structure morphogenesis	63	5.06	7	20.59	0.00111
GO:32989: cellular structure morphogenesis	40	3.213	6	17.65	0.000518
GO:902: cell morphogenesis	40	3.213	6	17.65	0.000518
GO:7399: nervous system development	48	3.855	6	17.65	0.00141
GO:65008: regulation of biological quality	56	4.498	6	17.65	0.00319
GO:48513: organ development	60	4.819	6	17.65	0.00455
GO:48518: positive regulation of biological process	93	7.47	6	17.65	0.036
GO:6915: apoptosis	94	7.55	6	17.65	0.0377
GO:12501: programmed cell death	95	7.631	6	17.65	0.0394
GO:8219: cell death	99	7.952	6	17.65	0.047
GO:48523: negative regulation of cellular process	99	7.952	6	17.65	0.047
GO:16265: death	99	7.952	6	17.65	0.047
GO:6457: protein folding	72	5.783	5	14.71	0.042
GO:30030: cell projection organization and biogenesis	18	1.446	4	11.76	0.00108
GO:48858: cell projection morphogenesis	18	1.446	4	11.76	0.00108
GO:32990: cell part morphogenesis	18	1.446	4	11.76	0.00108
GO:19725: cell homeostasis	36	2.892	4	11.76	0.0147
GO:42592: homeostatic process	37	2.972	4	11.76	0.0162
GO:6928: cell motility	50	4.016	4	11.76	0.0439
GO:51674: localization of cell	50	4.016	4	11.76	0.0439
GO:31175: neurite development	13	1.044	3	8.824	0.00442
GO:48666: neuron development	14	1.124	3	8.824	0.00552
GO:30003: cation homeostasis	17	1.365	3	8.824	0.00975
GO:30182: neuron differentiation	17	1.365	3	8.824	0.00975
GO:6873: cell ion homeostasis	18	1.446	3	8.824	0.0115
GO:30001: metal ion transport	18	1.446	3	8.824	0.0115
GO:50801: ion homeostasis	18	1.446	3	8.824	0.0115
GO:22008: neurogenesis	19	1.526	3	8.824	0.0134
GO:48699: generation of neurons	19	1.526	3	8.824	0.0134
GO:48878: chemical homeostasis	19	1.526	3	8.824	0.0134
GO:8284: positive regulation of cell proliferation	20	1.606	3	8.824	0.0154
GO:9966: regulation of signal transduction	29	2.329	3	8.824	0.0419
GO:42127: regulation of cell proliferation	29	2.329	3	8.824	0.0419
GO:7243: protein kinase cascade	30	2.41	3	8.824	0.0457
GO:9611: response to wounding	30	2.41	3	8.824	0.0457
Down-regulated proteins					
GO:8150: biological process	1,245	100	29	100	1
GO:44237: cellular metabolic process	824	66.18	24	82.76	0.0386
GO:43283: biopolymer metabolic process	389	31.24	15	51.72	0.0161
GO:61 nucleobase, nucleoside, nucleotide, and nucleic acid	337	27.07	14	48.28	0.011
GO:6397: mRNA processing	86	6.908	7	24.14	0.00263
GO:16071: mRNA metabolic process	101	8.112	7	24.14	0.0066
GO:6396: RNA processing	107	8.594	7	24.14	0.00907
GO:8380: RNA splicing	86	6.908	6	20.69	0.0119
GO:6259: DNA metabolic process	70	5.622	5	17.24	0.0201
GO:6281: DNA repair	23	1.847	3	10.34	0.0147
GO:6974: response to DNA damage stimulus	25	2.008	3	10.34	0.0185
GO:9719: response to endogenous stimulus	27	2.169	3	10.34	0.0228

TABLE III
The differentially expressed proteins related to the enriched biological processes

GO categories	Protein name (abbreviation)[a]
Up-regulated proteins	
Cell differentiation	SQSTM, RAC1, MAP1B, ENPL, CROP, NEUM, GAL1, TCTP, SCG2, S100A6, PROTA,[b] PAIRBP1[b]
Response to stress	RAC1, SQSTM, ENPL, DNJA1, CROP, AT1A1, SCG2, ANXA2, OXRP, PRDX6
Cell morphogenesis	RAC1, RADI, S100A6, ENOA, NEUM, MAP1B, MAGED1,[b] CRMP4[b]
Apoptosis (cell survival)	SQSTM, ENPL, TCTP, CROP, LEG1, SCG2, PAIRBP1,[b] MAGED1,[b] PROTA[b]
Homeostatic process	ENPL, AT1A1, PDI, TCTP,
Cell motility	MOES, AT1A1, SGTA, RAC1
Down-regulated proteins	
DNA and RNA metabolic process	HNRLL, SRR35, LSM8, FUBP2, HNRPF, SFRS2, PRP19, PCNA, H2B1C, H2B2A, FEN1
Other cellular metabolic process	VTDB, TBB4, GALK1, RL34, UBP48, CSK21, RLA0, IDHP, TIM13, PRPS2, DDC, RL6, APT

[a] The abbreviation of the protein name listed in Table I are shown in this table.
[b] These proteins were not annotated with the enriched biological processes, but they are speculated to be related to the biological process as reported in Refs. 34 and 35 for PAIRBP1, in Ref. 37 for PROTA, in Ref. 38 for MAGED1, and in Ref. 55 for CRMP4.

increased for 12 h and then gradually decreased. On the other hand, galectin-1 and ProTα expression levels peaked at 48 and 24 h, respectively. CRMP-4 and PAIRBP1 expression levels were constantly up-regulated during 12–72 h of NGF stimulation. The down-regulated protein, PCNA, was also consistently regulated in response to NGF (Fig. 4*A*). PAIRBP1 (34, 35), TCTP (36), ProTα (37), and MAGED1 (38) have been speculated to be functionally related to cellular differentiation and survival/apoptosis. We therefore sought to identify the roles of these proteins. Immunocytochemistry (ICC) showed that PAIRBP1 was expressed not only in the cytoplasm but also in the neurites, especially at the tips and junctions (Fig. 5*A*, *g* and *i*, *arrowheads*), whereas MAGED1 was expressed only in the cytoplasm (Fig. 5*D*, *g* and *i*). TCTP and ProTα were strongly expressed in the nucleus in response to NGF (Fig. 5, *B* and *C*, *g* and *i*, *arrows*). These results suggested that those proteins were involved in NGF-treated cellular responses.

Suppression of Differentially Expressed Proteins by siRNA Treatment—PAIRBP1, TCTP, ProTα, and MAGED1 were further analyzed using specific siRNAs to investigate their functions. siRNA-induced down-regulation was confirmed by Western blotting and ICC using their specific antibodies (Fig. 6, *A* and *B*) followed by a test of whether or not their suppression morphologically influenced the PC12 neurite formation. As expected, significant inhibition of the neurite formation was observed (Fig. 6*B*). Interestingly the suppression of MAGED1 caused aggregation of differentiating cells (Fig. 6, *B*, *IV* and *C*, *a*, and supplemental Movie 5). Furthermore we calculated the number and total length of neurites in differentiating cells and found that these measurements were certainly decreased by the suppression of each protein (Fig. 6*C*, *b* and *c*). In addition, apoptotic phenotypes were observed in NGF-stimulated cells treated with PAIRBP1, TCTP, or ProTα siRNA (Fig. 6*C*, *a* and supplemental Movies 2–4). We therefore observed the effects of the down-regulation of these proteins by siRNA on the survival of NGF-treated PC12 cells using PI staining for apoptotic cells coupled with nuclear staining by Hoechst33342. PAIRBP1, TCTP, or ProTα suppression caused a significant increase in PI-positive cells, whereas suppression of MAGED1 did not (Fig. 6*C*, *d* and *e*). These results suggested that, in PC12 cells, PAIRBP1, TCTP, ProTα, and MAGED1 regulate NGF-induced differentiation and that, except for MAGED1, they are involved in cell survival.

DISCUSSION

MS-based techniques targeting functional proteins in biological specimens have been developed to improve sensitivity, quantitation, and throughput. However, their application to biological study has not been satisfactory because their independent development has not met the needs of cell biologists and because of the lack of a sequential protocol and associated user-friendly analysis tools. Here we present a concise strategy consisting of sequential MS-based, *in silico*, and cell biological analyses to study the mechanisms of neuronal differentiation using PC12 cells.

Using MALDI-TOF-TOF and ESI-QqTOF in parallel, not only were certain proteins identified by both methods, but also unique proteins were independently identified by either of the methods. These data were combined to increase the number of identified proteins. It seemed important to know what kind of differences there were between the unique peptides identified by either of the systems. Previously Stapels and Barofsky (39) reported that the ESI system favored the identification of hydrophobic peptides whereas the MALDI system tended to lead to the identification of basic and aromatic peptides in the analysis of *E. coli* DNA-binding proteins. We noticed that the peptides identified by ESI-QqTOF had relatively higher theoretical pI values and molecular weights (pI = 6.46 and M_r = 1,694.4 on average) compared with those identified by MALDI-TOF-TOF (pI = 5.81 and M_r = 1,651.6 on average). The discrepancy, which seems contradictory, between our results and those of Stapels and Barofsky (39) may be explained by differences in sample, type of proteins analyzed, and the presence or absence of modification such as iTRAQ

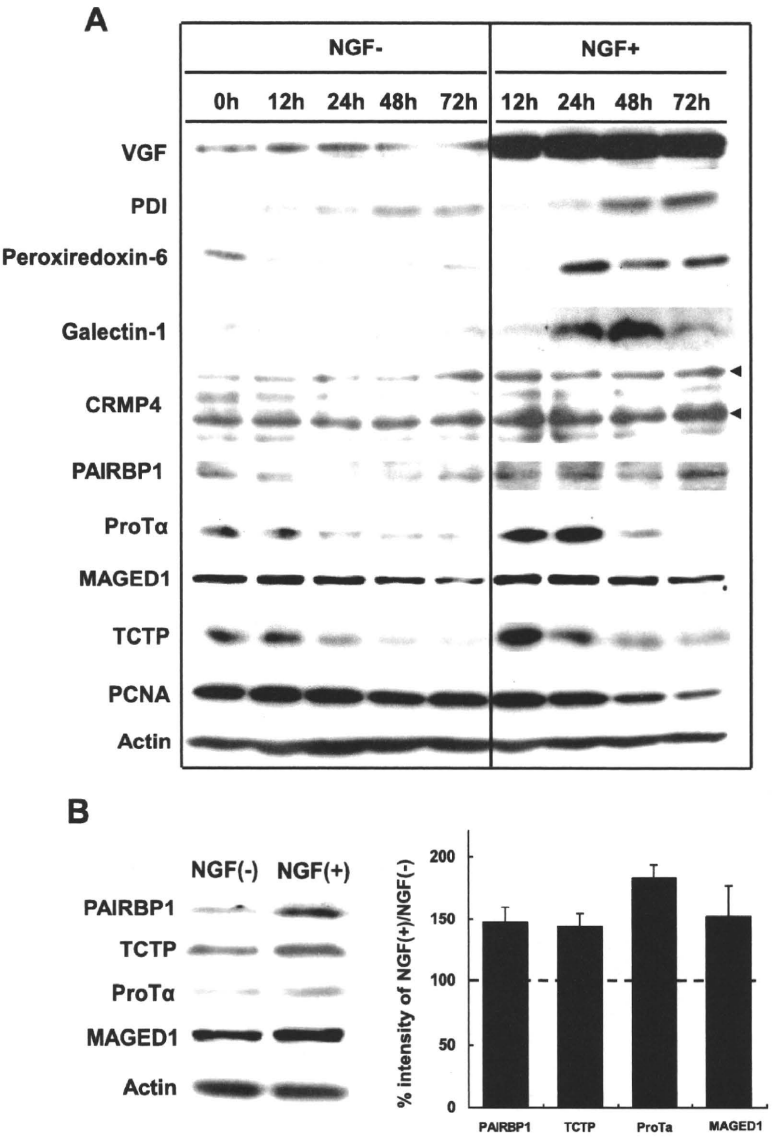

FIG. 4. **Immunoblot images of PC12 proteins differentially expressed in response to NGF stimulation.** Cell lysates were prepared at different time points as indicated. Actin expression was assessed for equal loading for all the proteins. *A*, the representative images are shown in four reproducible experiments. *Upper* and *lower arrowheads* show isoforms 1 and 2 of CRMP4, respectively. Some of those proteins showed a change in their expression levels even in untreated cells probably because of certain signals from collagen coated on the plates. *B*, Western blot images and quantification of the above four proteins PAIRBP1, TCTP, ProTα, and MAGED1 in NGF-stimulated PC12 cells. Cell lysates were prepared at 48 h after NGF stimulation. Actin expression was assessed for equal loading for all the proteins. The representative images are shown in four reproducible experiments. The ratios of percent intensities of the four proteins in NGF-stimulated *versus* untreated PC12 obtained from four separate identical experiments are shown in the histogram. *Error bars* represent S.D. The ratios were largely consistent with the corresponding iTRAQ ratios.

labeling. These results suggest that both MS systems may be complementary due to the biases of the two ionization systems and that analyses should be performed using both instruments to obtain more comprehensive information out of a given set of samples in a proteomics study.

In total, we analyzed 1,482 proteins with iTRAQ quantitation data of 4,899 proteins from 40,037 peptides identified by using the Mascot search engine (data not shown) in this study. To understand how our identification strategy covers the proteins expressed in PC12 cells, we analyzed the cellular component locations of all the identified proteins by the MANGO method and compared them with those of all human proteins listed in the Swiss-Prot database (20,332 entries, Release 57.2 of May 5, 2009) (supplemental Table 5). Of the 1,404 total identified human orthologs (PC12RPS), 1,231 were annotated with cellular component data. Of the latter, 758 (62%), 166 (13%), and 118 (10%) proteins were annotated with "cytoplasm," "mitochondrion," and "plasma membrane," respectively. On the other hand, among 16,530 human proteins from the Swiss-Prot database annotated with cellular component data, 7,106 (43%), 1,033 (6%), and 3,632 (22%) proteins were annotated with cytoplasm, mitochondrion, and plasma membrane, respectively. In the PC12RPS, the occurrence ratios of cytoplasm (62%) and mitochondrion (13%) were higher than those in the Swiss-Prot human proteins (43 and 6%, respectively), whereas the ratio of plasma membrane (10%) in PC12RPS was lower than that in the Swiss-Prot human proteins (22%). By combining this ratio of plasma membrane with the ratio of "organelle membrane" proteins (10.97%), the percentage of membrane proteins in the total proteins identified

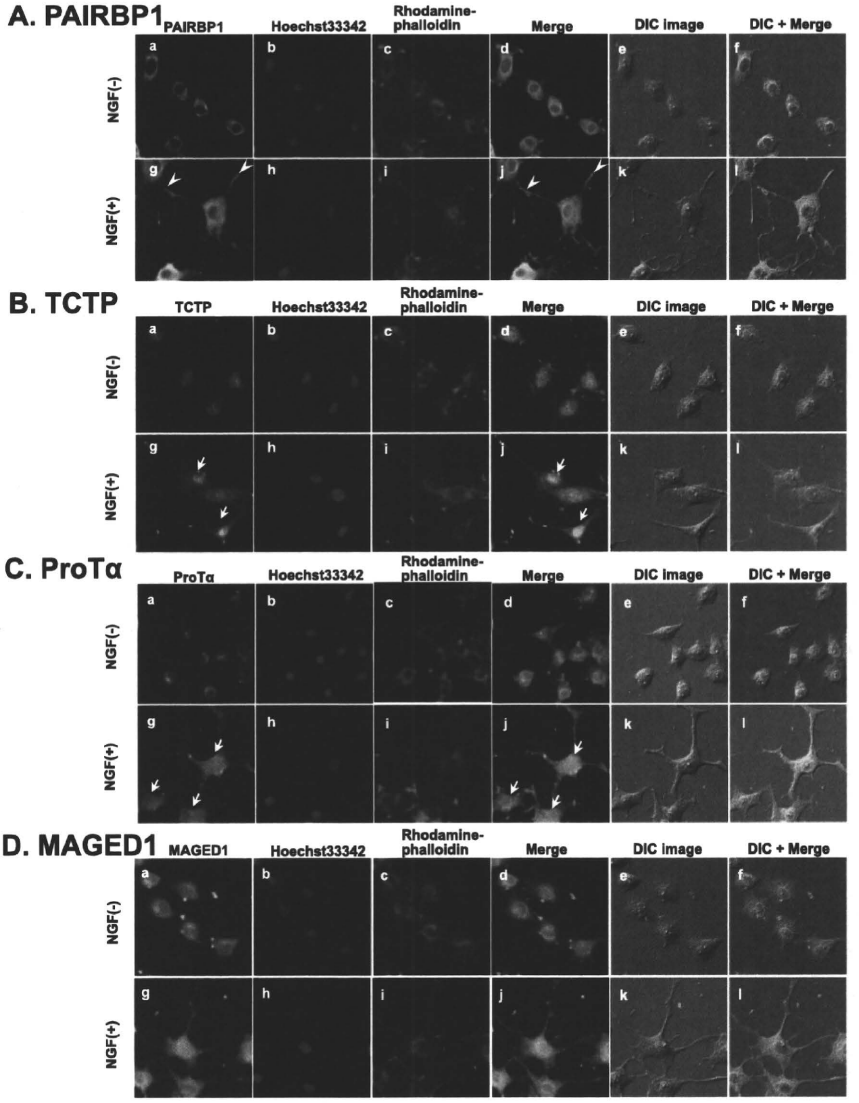

FIG. 5. **Analysis of NGF-responsive proteins by ICC.** PC12 cells were treated with NGF for 48 h. Cells were fixed and incubated with antibodies against the indicated proteins (*A*, PAIRBP1; *B*, TCTP; *C*, ProTα, and *D*, MAGED1) followed by detection with Alexa Fluor 488-labeled secondary antibodies (*a* and *g*) and observation with a fluorescence microscope. Nuclear and F-actin were stained with Hoechst33342 (*b* and *h*) and rhodamine-phalloidin (*c* and *i*), respectively. The merged images for *a*, *b*, *c* and *g*, *h*, *i* are shown in *d* and *j*, respectively. The merged images for *d*, *e* and *j*, *k* are shown in *f* and *l*. Differential interference contrast (*DIC*) images of PC12 cells in the same field are shown in *e* and *k*. *Arrowheads* indicate the PAIRBP1 expression in the neurite junctions and tips. *Arrows* indicate the TCTP and ProTα expression in the nucleus.

in our study becomes more than 20%. From these results, it is suggested that although cytoplasmic and mitochondrial proteins are largely favored in our method other components such as membrane and nuclear proteins can be also identified in significant numbers (supplemental Table 5).

From 1,482 proteins identified in iTRAQ quantitation, 72 differentially expressed proteins, including 39 up-regulated and 33 down-regulated, were extracted. The up-regulation of neurosecretory protein VGF (40), neuromodulin (41), chromogranin A (42), annexin A2 (43), peripherin (44), MAP1B (45), AHNAK (46), and secretogranin 2 (42) was observed as reported previously (Table II). Eighteen proteins in our results also corresponded to NGF-responsive genes in cDNA microarray data of Dijkmans *et al.* (23) (Table II) that coincided with our results, showing the confidence and reliability of our methods. Sixty-four proteins were heretofore unreported (Table II). The majority were cytoskeletal organizing components, such as moesin, radixin, MAP1B, annexin A2, peripherin, CRMP-4, RAC1, keratin-8, and keratin-18, whose changes in expression suggested roles for them in the cytoskeletal reorganization for cellular motility and morphogenesis. Interestingly PCNA and flap endonuclease 1 are both required for DNA replication, and both histones H2A and H2B are nucleosome components, all of which were down-regulated by NGF treatment. These results suggested that the down-regulation of these proteins was a factor in the arrest of cell division and the initiation of PC12 neuronal differentiation.

Further biological and functional interpretation of the above proteins was performed by proteomics GO analysis using the GO annotation and analysis tool. Here we encountered two problems. First, unlike microarray data, proteomics data con-

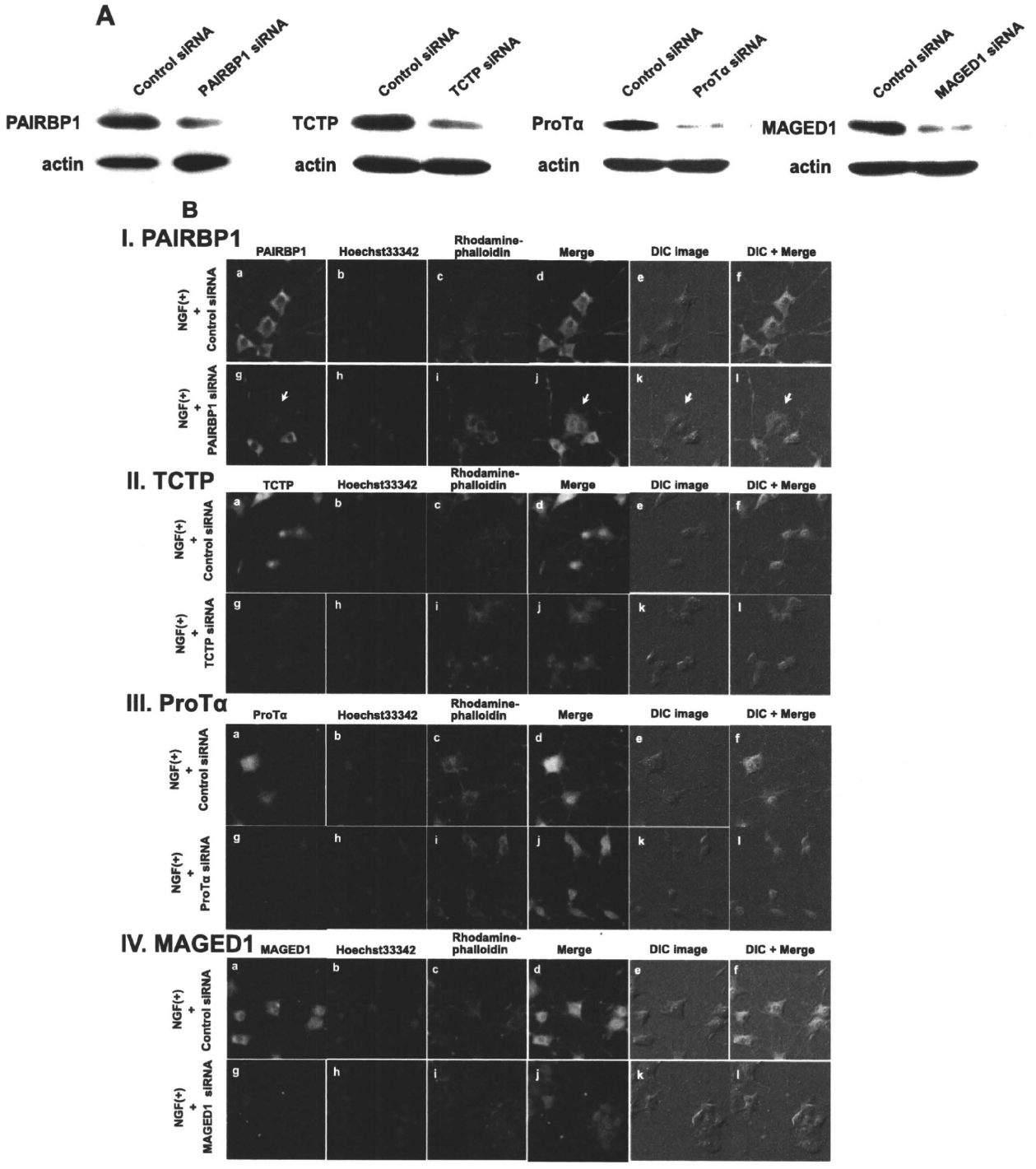

FIG. 6. **The effects caused by the suppression of the NGF-inducible proteins on PC12 cell differentiation.** *A*, the cells were transfected with siRNA for each NGF-inducible protein or control siRNA for 24 h and then treated with NGF for 48 h. Immunoblot images were taken after treatment with each siRNA of the protein. Down-regulation of these proteins was confirmed. *B*, the cells were transfected with siRNA for each NGF-inducible protein or control siRNA for 24 h and then treated with NGF for 48 h. Cells were fixed and incubated with the antibodies against the indicated proteins (*I*, PAIRBP1; *II*, TCTP; *III*, ProTα; and *IV*, MAGED1) followed by detection with Alexa Fluor 488-labeled secondary antibodies and observation with a fluorescence microscope (*a* and *g*). Nuclear and F-actin were stained with Hoechst33342 (*b* and *h*) and rhodamine-phalloidin (*c* and *i*), respectively. The merged images for *a*, *b*, *c* and *g*, *h*, *i*, are shown in *d* and *j*, respectively. The merged images